© 2022. Published by The Company of Biologists Ltd | Journal of Cell Science (2022) 134, jcs253591. doi:10.1242/jcs.253591

RESEARCH ARTICLE

Smaug1 membrane-less organelles respond to AMPK and mTOR and affect mitochondrial function

Ana J. Fernández-Alvarez[1,2,*], María Gabriela Thomas[1,2,*], Malena L. Pascual[1,2], Martín Habif[3], Jerónimo Pimentel[1,2], Agustín A. Corbat[3], João P. Pessoa[4], Pablo E. La Spina[1,2], Lara Boscaglia[1], Anne Plessis[5], Maria Carmo-Fonseca[4], Hernán E. Grecco[3], Marta Casado[6] and Graciela L. Boccaccio[1,2,7,‡]

ABSTRACT

Smaug is a conserved translational regulator that binds numerous mRNAs, including nuclear transcripts that encode mitochondrial enzymes. Smaug orthologs form cytosolic membrane-less organelles (MLOs) in several organisms and cell types. We have performed single-molecule fluorescence *in situ* hybridization (FISH) assays that revealed that SDHB and UQCRC1 mRNAs associate with Smaug1 bodies in U2OS cells. Loss of function of Smaug1 and Smaug2 (also known as SAMD4A and SAMD4B, respectively) affected both mitochondrial respiration and morphology of the mitochondrial network. Phenotype rescue by Smaug1 transfection depends on the presence of its RNA-binding domain. Moreover, we identified specific Smaug1 domains involved in MLO formation, and found that impaired Smaug1 MLO condensation correlates with mitochondrial defects. Mitochondrial complex I inhibition upon exposure to rotenone, but not strong mitochondrial uncoupling upon exposure to CCCP, rapidly induced the dissolution of Smaug1 MLOs. Metformin and rapamycin elicited similar effects, which were blocked by pharmacological inhibition of AMP-activated protein kinase (AMPK). Finally, we found that Smaug1 MLO dissolution weakens the interaction with target mRNAs, thus enabling their release. We propose that mitochondrial respiration and the AMPK–mTOR balance controls the condensation and dissolution of Smaug1 MLOs, thus regulating nuclear mRNAs that encode key mitochondrial proteins.

This article has an associated First Person interview with the first authors of the paper.

[1]Fundación Instituto Leloir (FIL), Av Patricias Argentinas 435, C1405BWE Buenos Aires, Argentina. [2]Instituto de Investigaciones Bioquímicas de Buenos Aires (IIBBA) - Consejo Nacional de Investigaciones Científicas y Tecnológicas (CONICET), Av Patricias Argentinas 435, C1405BWE Buenos Aires, Argentina. [3]Department of Physics, Facultad de Ciencias Exactas y Naturales (FCEN), University of Buenos Aires, and IFIBA, CONICET, C1428EHA Buenos Aires, Argentina. [4]Instituto de Medicina Molecular João Lobo Antunes, Faculdade de Medicina, Universidade de Lisboa, Avenida Professor Egas Moniz, 1649-028, Lisboa, Portugal. [5]Institut Jacques Monod, CNRS, UMR 7592, University Paris Diderot, Sorbonne Paris Cité, F-75205 Paris, France. [6]Instituto de Biomedicina de Valencia, IBV-CSIC, Valencia 46010, Spain, and Centro de Investigación Biomédica en Red de Enfermedades Hepáticas y Digestivas (CIBERehd), Madrid 28029, Spain. [7]Department of Molecular and Cellular Biology and Physiology (FBMyC), Facultad de Ciencias Exactas y Naturales (FCEN), University of Buenos Aires, C1428EHA Buenos Aires, Argentina.
*These authors contributed equally to this work

‡Author for correspondence (gboccaccio@leloir.org.ar)

A.J.F., 0000-0002-5296-5678; M.G., 0000-0001-6164-8044; M.L.P., 0000-0002-9815-1880; M.H., 0000-0001-7548-4247; A.A.C., 0000-0001-8068-3486; M.C., 0000-0002-3402-7143; H.E.G., 0000-0002-1165-4320; M.C., 0000-0001-6457-4650; G.L.B., 0000-0003-1349-898X

Handling Editor: David Stephens
Received 9 September 2020; Accepted 15 November 2021

KEY WORDS: Smaug, Membrane-less organelles, Processing bodies, Mitochondria, Metformin, AMPK, UQCRC1

INTRODUCTION

Smaug orthologs bind transcripts that contain a variety of stem-loops termed Smaug recognition elements (SREs). Several unbiased screens in *Drosophila* have allowed the identification of thousands of target mRNAs that are involved in widely diverse cellular processes. mRNA regulation by Smaug has been addressed in a few cases and it may involve translational repression and/or decay (Amadei et al., 2015b; Aviv et al., 2006; Baez and Boccaccio, 2005; Cao et al., 2020; Chartier et al., 2015; Chen et al., 2014a; Eichhorn et al., 2016; Johnson and Donaldson, 2006; Laver et al., 2012; Nelson et al., 2004; Niu et al., 2017; Oberstrass et al., 2006; Pinder and Smibert, 2013; Rouget et al., 2010; Semotok et al., 2005, 2008; She et al., 2017; Tadros et al., 2007). Both insect and vertebrate Smaug form membrane-less organelles (MLOs) termed Smaug foci or Smaug bodies, which contain repressed mRNAs. Smaug bodies have been identified in mammalian neuroblasts, hippocampal dendrites, fly embryo and adult muscle, and are distinct from processing bodies (PBs), a well-known type of MLO that also contain repressed mRNAs (Amadei et al., 2015b; Baez and Boccaccio, 2005; Baez et al., 2011; Chartier et al., 2015; Rouget et al., 2010; Sachdev et al., 2019). The formation of MLOs and related molecular condensates is thought to involve liquid–liquid phase separation (LLPS) processes driven by multiple non-covalent interactions, which remain unknown in the case of Smaug bodies (Courchaine et al., 2016; Guo and Shorter, 2015; Perez-Pepe et al., 2018; Sachdev et al., 2019; Van Treeck et al., 2018). The molecular consequences of Smaug body formation are incipiently described. In yeast, the condensation of the Smaug ortholog Vts1p facilitates the degradation of target mRNAs (Chakravarty et al., 2020). In mammalian neurons, Smaug1 body dissolution is linked to mRNA release and translational activation of dendritic mRNAs (Baez et al., 2011; Luchelli et al., 2015).

The dysregulation of Smaug orthologs in different organisms and tissues leads to a wide diversity of phenotypes. *Drosophila* Smaug loss of function provokes embryo defects due to the abnormal expression of maternal mRNAs. In addition, fly Smaug binds numerous mRNAs that encode glycolytic and mitochondrial enzymes (Chartier et al., 2015; Chen et al., 2014a; Schatton and Rugarli, 2018; Tadros et al., 2007). The two mammalian paralogs termed Smaug1 and Smaug2 (also known as Samd4A and Samd4B, respectively) are involved in neuron differentiation, synapse plasticity and bone development (Amadei et al., 2015b; Baez et al., 2011; Luchelli et al., 2015; Niu et al., 2017). Overexpression of *Drosophila* or mammalian Smaug1 in muscular cells suppress myotonic dystrophy-1 (MD1) (de Haro et al., 2013). Independent work in *Drosophila* and mammalian systems has identified fly

Journal of Cell Science (2022) 134, jcs253591. doi:10.1242/jcs.253591

Smaug and mouse Smaug1 as enhancers of mitochondrial defects caused by aberrant mRNA polyadenylation, where the most affected mRNAs encode proteins of the electron transport chain (ETC) and were enriched in SREs (Chartier et al., 2015). In addition, a point mutation in murine Smaug1, termed Supermodel, generates a complex phenotype characterized by leanness, resistance to fat intake-induced obesity, reduced muscle and adipose tissue, and abnormal morphology of both myofibers and adipocytes (Chen et al., 2014b). A number of mRNAs related to mitochondrial uncoupling are upregulated in Supermodel mice, and whether the effect involves direct binding of these transcripts to Smaug is unknown. Finally, studies in yeast have shown that Vts1p is involved in nutrient sensing (Chakravarty et al., 2020; She et al., 2017). Thus, a connection between Smaug and the energetic metabolism appears to be conserved from yeast to animals.

mRNAs that encode the mitochondrial enzymes succinate dehydrogenase subunit B (SDHB) and ubiquinol-cytochrome *c* reductase core protein 1 (UQCRC1) were previously reported to bind fly Smaug in both embryonic and adult *Drosophila* tissues (Chartier et al., 2015; Chen et al., 2014a). Here, we show that mammalian Smaug1 MLOs interact with both SDHB and UQCRC1 mRNAs. Specifically, single-molecule fluorescence *in situ* hybridization (FISH) revealed that SDHB and UQCRC1 mRNAs associate with Smaug1 bodies in U2OS cells. In addition, loss of function of Smaug1 and Smaug2 affected both mitochondrial respiration and mitochondrial network complexity. Phenotype rescue by Smaug1 transfection depended on the presence of the RNA-binding domain. Moreover, we identified specific Smaug1 domains involved in MLO formation, and found that Smaug1 deletion mutants with defective MLO formation fail to rescue the phenotype. In addition, we investigated whether mitochondrial activity could affect Smaug1 MLO dynamics and found that complex I inhibition upon exposure to rotenone rapidly induced Smaug1 body dissolution, whereas strong mitochondrial uncoupling upon treatment with carbonyl cyanide 3-chlorophenylhydrazone (CCCP) had no effect. Furthermore, inhibition of mechanistic target of rapamycin (mTOR) by rapamycin similarly induced Smaug1 MLO dissolution, and exposure to metformin – an inhibitor of complex I and activator of AMP-activated protein kinase (AMPK) widely used for the treatment of type II diabetes – immediately induced Smaug1 MLO dissolution and mRNA release. In addition, the effect induced by rotenone, metformin or rapamycin was fully blocked by Compound C, a known AMPK inhibitor. Finally, disruption of polysome assembly through treatment with puromycin blocked the dissolution of Smaug1 MLOs triggered by these stimuli. Altogether, these observations suggest that Smaug1 MLOs respond to mitochondrial activity and the AMPK–mTOR balance, thus enabling the regulated release of key transcripts.

RESULTS

SDHB and UQCRC1 mRNAs associate to Smaug1 membrane-less organelles

Smaug orthologs are expressed in several mammalian cell lines (Fernández-Alvarez et al., 2016) and as expected, we found that Smaug1 forms cytosolic puncta in U2OS cells (Fig. 1A). Smaug1 bodies were present in 70–80% of cells (five independent experiments, $n \geq 200$ cells in each replicate). Their size and distribution reminded us of that of PBs; however, we found that Smaug1 bodies did not colocalize with PBs identified by DCP1A staining (Fig. 1A), as previously reported in neurons (Baez et al., 2011). In addition, Smaug1 bodies dissolved upon exposure to cycloheximide, suggesting that they can release translation-competent mRNAs. Both the number of cells with Smaug-1 bodies and the number of Smaug-1 bodies per cell were reduced upon treatment with cycloheximide (Fig. 1B).

Transfected Smaug1–EYFP and Smaug1–V5 similarly condense in cytosolic bodies (Baez and Boccaccio, 2005; Baez et al., 2011) that are comparable in size and distribution to endogenous Smaug1 bodies (Fig. 1C). Smaug1–EYFP bodies do not contain small ribosomal subunits, indicating that they are not stress granules (SGs) (Fig. S1A). In addition, Smaug1 bodies did not contain ubiquitin, a marker of aggregates of abnormal or damaged protein (Fig. S1A). Thus, transfection of Smaug1 is a reliable strategy for further studies. Next, we performed real time microscopy and found that Smaug1–EYFP bodies are highly dynamic. Smaug1–EYFP bodies sporadically fuse, a feature characteristic of MLOs (Fig. 1C; Movie 1).

Drosophila Smaug binds to several nuclear transcripts that encode mitochondrial enzymes (Bruzzone et al., 2020; Chartier et al., 2015; Chen et al., 2014a; Tadros et al., 2007) (Table S1) and among many other putative mammalian targets, we analyzed the mRNAs of NADH:ubiquinone oxidoreductase subunit A10 (NDUFA10), SDHB and UQCRC1. We transfected and pulled-down Smaug1 fused to a V5–SBP double tag and evaluated the co-purification of NDUFA10, SDHB and UQCRC1 mRNAs by reverse transcription real-time quantitative PCR (RT-qPCR) (Fig. 1D). Both SDHB and UQCRC1 mRNAs were recovered in the V5–SBP–Smaug1 pull-down material. In contrast, NDUFA10 mRNA was not significantly enriched, and its recovery was similar to that of PP1A mRNA. Smaug1 ΔEIII, a natural splicing variant that forms similar cytosolic bodies (Fernández-Alvarez et al., 2016) showed a similar binding profile. The control construct V5–SBP–MBP did not pull down these transcripts (Fig. 1D; Fig. S1B). These results are comparable to observations reported in *Drosophila*, where SDHB mRNA is enriched fourfold in fly Smaug pull-downs and NDUFA10 mRNA is among the transcripts with lower recovery rates (Chartier et al., 2015). Based on previous work in *Drosophila*, we speculate that additional mRNAs that encode mitochondrial proteins might bind mammalian Smaug1, which remains to be investigated (Bruzzone et al., 2020; Chartier et al., 2015; Chen et al., 2014a).

Next, we used single-molecule FISH to simultaneously detect SDHB mRNA, UQCRC1 mRNA and Smaug1–EYFP bodies (Fig. 1E). The association of these mRNAs with Smaug1–EYFP bodies was manually assessed, and we found that a statistically significant fraction of Smaug1 bodies contained or contacted SDHB or UQCRC1 mRNA puncta (Fig. 1F). Manders' colocalization analysis of original and randomized images similarly indicated that SDHB mRNA and UQCRC1 mRNA associated to Smaug1-EYFP bodies (Fig. 1F). In addition, the presence of SDHB and UQCRC1 mRNAs in a single Smaug1–EYFP body was not mutually exclusive. By contrast, the co-occurrence of the two transcripts was higher than that predicted as independent events ($0.24 \times 0.34 = 0.08$ versus 0.15 in Fig. 1F).

Finally, we analyzed whether Smaug1 MLOs contact mitochondria identified by TOM20 (also known as TOMM20) immunostaining (Fig. 1G,H). The frequency of contacts was assessed by an automatized analysis (see Materials and Methods), and was moderately higher than the one calculated in randomized images (Fig. 1F) (French et al., 2016). We have previously shown that Smaug1 and Smaug2 colocalize in cytosolic bodies (Fernández-Alvarez et al., 2016), and here we analyzed, by western blotting, the distribution of Smaug1 and Smaug2 in cellular fractions. Both Smaug1 and Smaug2 were mostly cytosolic and did not co-purify with mitochondria. This result further

Journal of Cell Science (2022) 134, jcs253591. doi:10.1242/jcs.253591

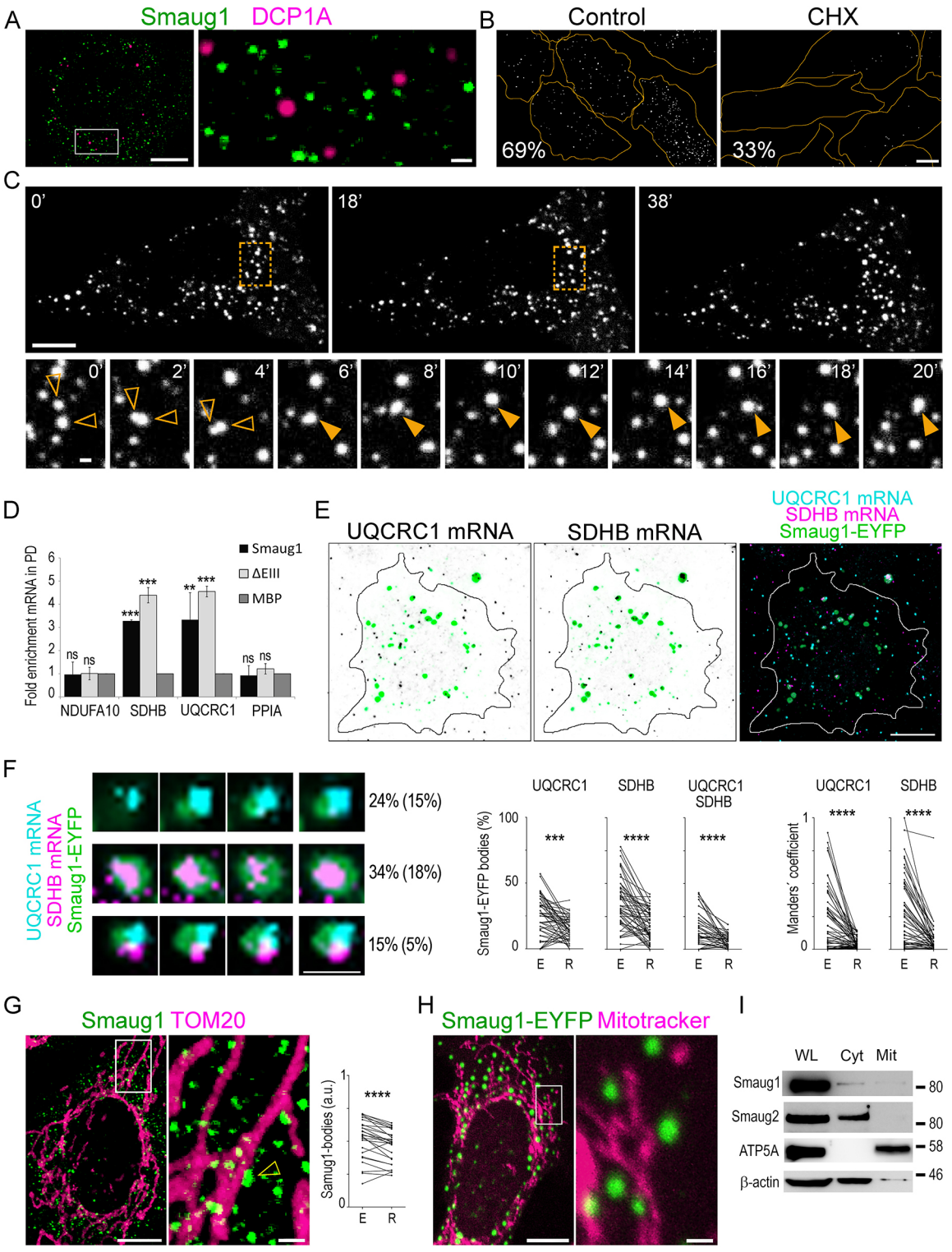

Fig. 1. See next page for legend.

suggests that Smaug1 and Smaug2 MLOs sporadically contact the mitochondrial surface and do not remain tethered.

Smaug1 and Smaug2 knockdown impairs mitochondrial respiration

We investigated the effect of the double knockdown of Smaug1 and Smaug2 (Smaug1+2 double KD), which were efficiently silenced by specific siRNAs (siSmaug1 and siSmaug2) (Fig. 2A). We analyzed the expression of UQCRC1 by immunofluorescence. Single-cell analysis indicated that UQCRC1 protein levels were highly variable and importantly, Smaug1+2 double KD cells frequently showed higher UQCRC1 levels than control cells (Fig. 2B). On average, the UQCRC1 signal increased 1.5 times upon Smaug1+2 double KD. Taken together with the results shown in Fig. 1D–F, these observations suggest that UQCRC1 mRNA is repressed by Smaug1 and/or Smaug2. Western blot analysis

Fig. 1. Smaug1 bodies contain mRNAs that encode mitochondrial enzymes. (A) Immunofluorescence for DCP1A and Smaug1 in U2OS cells. (B) Cells were exposed to cycloheximide for 1 h, and the percentage of cells with Smaug1 bodies is indicated. Cell contours (orange) were drawn as described in the Materials and Methods. A representative experiment out of three is shown, where 200 cells from duplicate coverslips were analyzed. (C) Smaug1–EYFP was recorded in live cells. In magnified images below, two bodies (empty arrowheads) start merging at 2 min and remain fussed (full arrowhead). Fusion with a third body starts at 18 min. Three independent experiments showed a similar behavior. (D) RNA pull-down. Smaug1, Smaug1 ΔEIII or MBP, all of them tagged with V5-SBP were pulled down and the indicated transcripts were analyzed by RT-qPCR. Three independent experiments were performed and mean values of the pull-down (PD)/input ratio for each transcript normalized to RpLp0 mRNA are plotted. Error bars, s.d. Expression levels and recovery of V5-SBP-tagged constructs were analyzed by western blotting (Fig. S1B). (E) Single-molecule FISH for SDHB and UQCRC1 mRNAs was performed in cells expressing Smaug1–EYFP. Cell contours (solid line) was drawn as described in the Materials and Methods. A representative experiment out of two is shown. (F) Three adjacent confocal slices and maximal projection of three representative Smaug1–EYFP bodies are depicted. The percentage of Smaug1–EYFP bodies containing or contacting only SDHB mRNA, only UQCRC1 mRNA, or both transcripts was assessed manually. Image randomization was performed as described in Materials and Methods and values from randomized images are in brackets. The experimental values (E) and the corresponding averaged random values (R) obtained by both manual assessment and according to Manders' are plotted. 50 ROIs including 751 Smaug1-EYFP bodies from 13 cells from 4 coverslips from two independent stainings were analyzed. Statistical significance was analyzed by paired two-tailed *t*-test. (G) Smaug1 and TOM20 were immunostained. The fraction of Smaug1 bodies contacting mitochondria (arrowheads) was analyzed as indicated in Materials and Methods. Experimental values for 26 ROIs and the corresponding average random values are plotted. A representative experiment out of three is shown. a.u., arbitrary units. (H) Smaug1–EYFP-transfected U2OS cells were live-stained with MitoTracker™ Red CMXRos. (I) The indicated proteins were analyzed by western blot of whole lysate (WL), cytosolic (Cyt) and mitochondrial (Mit) extracts. Two independent fractionation experiments were performed and a representative western blot is shown. Scale bars: 10 µm for whole cells in A, B, C, E, G, H; 1 µm for magnified images in C, F, G, H. ***P*<0.01; ****P*<0.001; *****P*<0.0001; ns, not significant (one-way ANOVA and Tukey post-test except where indicated).

similarly indicated a moderate increase of UQCRC1 protein levels upon Smaug1+2 double KD (Fig. S2A). The levels of NDUFB8, SDHB, UQCRC2, MTCO1 and ATP5A were also analyzed by western blotting, and no significant changes were found upon Smaug1+2 KD (Fig. S2A).

In addition, we measured the respiratory capacity of intact or permeabilized cells using high-resolution respirometry. We used a protocol termed (SUIT)-RP2, which allows the measurement of the F-pathway, the electron transport capacity and the maximum oxidative phosphorylation (OXPHOS) (Doerrier et al., 2018). We found significant changes in permeabilized cells (Fig. 2C), whereas no effects were observed in intact cells (Fig. S2B). Routine endogenous respiration – which depends on intracellular substrates – remained unchanged upon Smaug1+2 double KD, in accordance with the lack of effect observed in intact cells. In contrast, oxygen flux through fatty acid oxidation was reduced upon Smaug1 and Smaug2 double KD (Fig. 2C). A moderate reduction in oxygen flow was observed after activation of the N-pathway with malate [F(N)]. The effect was more significant in the presence of malate, pyruvate and glutamate [FN(PGM)], and stronger upon the addition of succinate (FNS), suggesting defective complex I and II activities. Oxygen flow increased significantly in both control and KD cells after addition of glycerophosphate, indicating that glycerophosphate dehydrogenase shuttle (FNSGp) is functional in both cases, with almost normal maximum respiratory capacity and oxygen flow after inhibition of complex I (FNSGpe; SGpe). Finally, complex IV activity was not affected by Smaug1+2 double KD [control non-targeting siRNA (siNT), 168; siSmaug1+2, 164 pmol/s×million cells×mtDNA, see Materials and Methods]. Taken together, these observations indicate decreased succinate-activated respiration upon Smaug1 and Smaug2 double KD. In addition, we studied the effect of Smaug1+2 KD on mitochondrial membrane potential by JC-1 staining. Cells treated with the strong depolarizing agent CCCP were analyzed in parallel. Silencing of Smaug1+2 did not significantly affect mitochondrial membrane potential (Fig. 2D,E).

Mitochondrial network disruption upon Smaug1 and Smaug2 knockdown

Collectively, the above observations indicate that Smaug1+2 KD affects OXPHOS activity without provoking serious mitochondrial damage. The mitochondrial network is dynamically regulated in connection with mitochondrial respiration, and we analyzed its overall morphology by TOM20 staining (Fig. 3). We classified the cells into two groups, those with short mitochondria and those with elongated and branched mitochondria. Single or double KD of Smaug1 and/or Smaug2 significantly reduced the complexity of the mitochondrial network (Fig. 3A). Between 50 and 80% of untreated cells showed elongated mitochondria, and this number was reduced to less than half upon Smaug1 and Smaug2 double KD. Single KD of either Smaug1 or Smaug2 elicited a statistically significant effect, yet not as strong as the double KD (Fig. 3B). Mitochondria were also analyzed by live-cell staining with MitoTracker™ Red CMXRos, and similar results were obtained (Fig. S3A).

The mitochondrial DNA content relative to the nuclear DNA content was evaluated by qPCR of the mitochondrial gene cytochrome *c* oxidase 2 and the nuclear gene SDHA, and similar values were observed in all conditions (siNT 1±0.3; siSmaug1, 1.1±0.3; siSmaug2 0.9±0.1; siSmaug1+siSmaug2 1.1±0.3; mean±s.d., n=3) indicating that mitochondrial mass was not affected. Relevantly, in addition to UQCRC1 and SDHB mRNAs, Smaug orthologs bind numerous RNAs key for mitochondrial function, including several ETC components, mitochondrial ribosomal proteins, tRNA modifying enzymes, transporters and protein folding factors (Chartier et al., 2015; Chen et al., 2014a). We speculate that the collective dysregulation of several mRNAs under Smaug control is causative of the phenotype described here.

The morphology of the mitochondrial network depends on the balance between mitochondrial fusion and fission. Reduced fusion is linked to changes in the proteolytic cleavage of mitochondrial dynamin like GTPase (Opa1), and in the levels of mitofusin 1 (Mfn1) and mitofusin 2 (Mfn2). We analyzed these molecular markers upon Smaug1 and Smaug2 double KD and after exposure to mitochondrial inhibitors (Fig. 3C,D). We found that both Opa1 and Mfn2 remained unaltered upon the Smaug1 and Smaug2 double KD (Fig. 3D). In addition, Opa1 and Mfn2 remained unaltered upon exposure to rotenone, which inhibits complex I and triggers a moderate fragmentation of the mitochondrial network (Fig. 3C,D) (Toyama et al., 2016). In contrast and as expected, CCCP elicited a strong response. Levels of the Opa1 long (L) fragment relative to levels of the short (S) fragment were reduced, and Mfn2 levels were downregulated. All this correlated with decreased membrane potential (Fig. 2D,E) and strong mitochondrial network fragmentation upon exposure to CCCP (Fig. 3C).

To further assess the functionality of the fusion machinery, we analyzed a specific response that depends on Opa1 and Mfn, termed stress-induced mitochondrial hyperfusion (SIMH) (Ehses et al., 2009; Tondera et al., 2009) (see Materials and Methods). We found that SIMH was not altered upon Smaug1+2 KD. The fraction of siNT-

Journal of Cell Science (2022) 134, jcs253591. doi:10.1242/jcs.253591

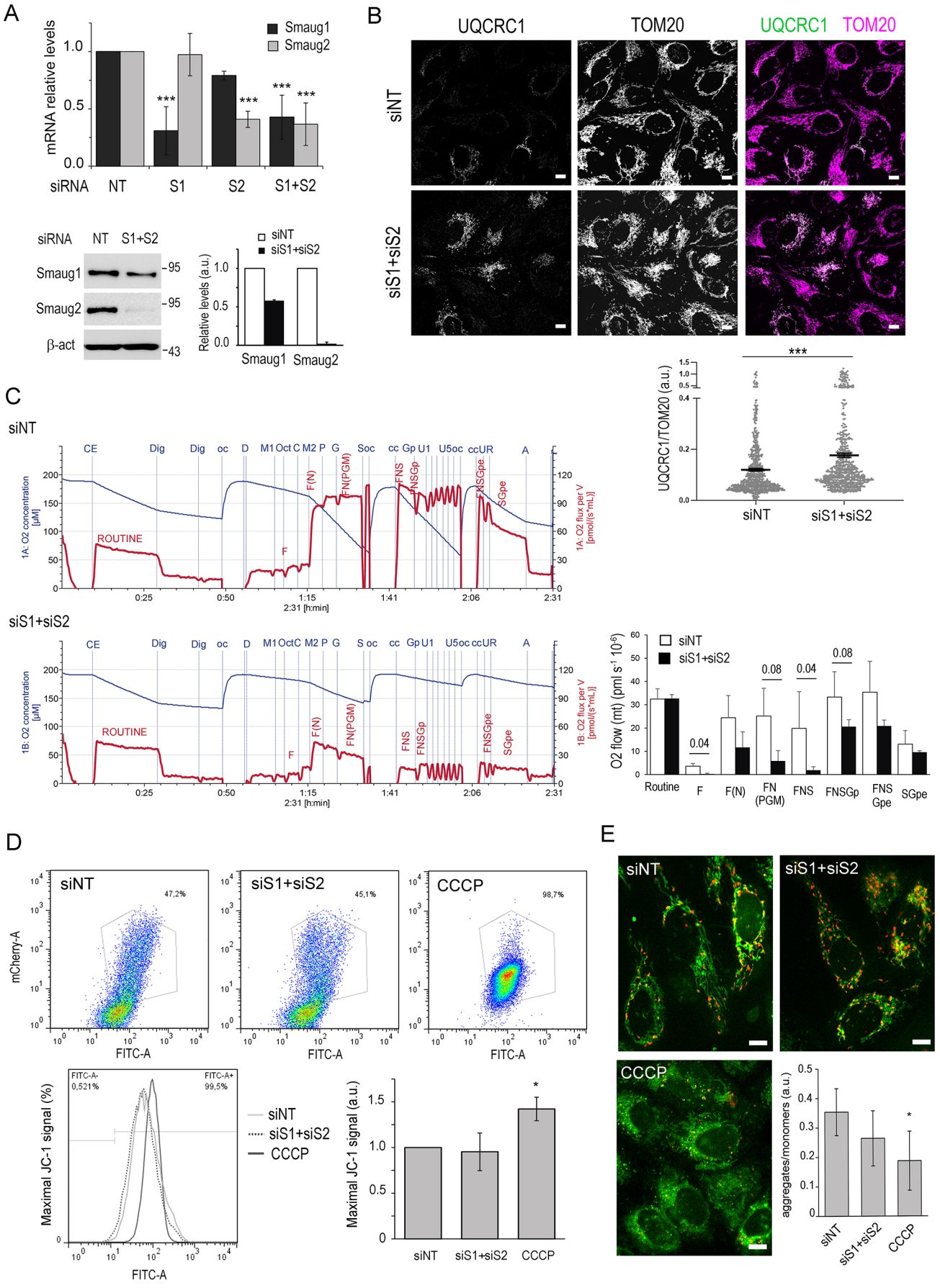

Fig. 2. See next page for legend.

Journal of Cell Science

Journal of Cell Science (2022) 134, jcs253591. doi:10.1242/jcs.253591

Fig. 2. Respiratory defects upon Smaug1 and Smaug2 knockdown. (A) U2OS cells were treated with siRNAs against Smaug1 (S1) and/or Smaug2 (S2), or a non-targeting siRNA (NT). Smaug1 and Smaug2 mRNA levels were analyzed by RT-qPCR in three independent experiments and a representative replicate is shown. Smaug1 and Smaug2 protein levels were analyzed by western blot in two independent experiments and average values are indicated. (B) UQCRC1 protein levels were analyzed by immunofluorescence in U2OS cells treated with the indicated siRNAs. The intensity of UQCRC1 signal relative to TOM20 was determined in more than 200 cells from duplicate coverslips from two independent experiments. (C) High-resolution respirometry in permeabilized cells. Top, representative traces of oxygen concentration (blue) and oxygen flow (red). The addition of digitonin (Dig), ADP (D), 0.1 mM malate (M1), octoanylcarnitine (Oct), cytochrome c (C), 2 mM malate (M2), pyruvate (P), glutamate (G), succinate (S), phosphoglycerate (Gp), CCCP (U1-U5), rotenone (R) and antimycin A (A) is indicated with dotted lines as well as re-oxygenation and closing of the chambers (oc and cc, respectively). Sections reflecting OXPHOS fingerprints are labeled. Right, the averaged mean oxygen flow per million cells (±s.e.m.) from three independent experiments performed in duplicate is plotted. Statistical significance was calculated as described in Materials and Methods. *P* values lower than 0.1 are indicated. (D,E) Mitochondrial potential was analyzed using JC-1 dye. (D) Flow cytometry analysis of JC-1 aggregates (red) and monomers (green). Bottom right, JC-1 monomers signal was quantified using geometric median from three independent experiments and plotted as fold change ±s.e.m. (E) JC-1-aggregates (magenta) and monomers (green) were analyzed by confocal live microscopy. The proportion of aggregates/monomers calculated as the average intensity ratio from ten fields from a representative experiment out of two is plotted. Scale bars: 10 µm. **P*<0.05; ****P*<0.001 [paired two-tailed Student's t-test (D); one-way ANOVA and Tukey post-test (A,B,C,E)].

treated cells that showed elongated mitochondria increased from 50% to 77% upon SIMH induction. Smaug1+2 KD cells also responded significantly and the proportion of cells with elongated mitochondria increased from 21% to 74% after SIMH induction (Fig. 3E). Collectively, these observations indicate that the mitochondria fusion machinery is fully functional in Smaug1+2 KD cells.

Mitochondrial fission is actively promoted by the recruitment of dynamin-1-like protein (DRP1, also known as DNM1L) to the mitochondrial surface (Hoppins et al., 2007; Pitts et al., 1999). We analyzed the recruitment of DRP1 by immunofluorescence and western blotting. We found that the number of DRP1 puncta associated with the mitochondria doubled compared to the basal levels upon Smaug1+2 KD (Fig. 3F). In addition, western blot analysis indicated that DRP1 levels increased significantly in the mitochondrial fraction upon Smaug1+2 KD (Fig. 3G). Finally, Smaug1+2 double KD did not induce AMPK phosphorylation (Fig. S3B), thus suggesting that mitochondrial fission factor (MFF), which is an AMPK-dependent DRP1 receptor (Toyama et al., 2016), is unlikely to be involved.

Taken together with the above results, these observations suggest that Smaug1+2 KD activates mitochondrial fission, likely as a consequence of altered mitochondrial respiration. In the following studies, we analyzed changes in the mitochondrial network to further investigate the relevance of Smaug1 MLO formation.

First, we analyzed whether the mitochondrial phenotype provoked by Smaug1 and Smaug2 double KD is rescued by transfection of Smaug1 (Fig. 4). We found that this is the case and, in addition, the splicing variant ΔEIII, which has similar RNA binding and repression capacity (Fig. 1; Fernández-Alvarez et al., 2016), also rescued the mitochondrial phenotype (Fig. 4). Altogether, these observations suggest that the three mammalian Smaug isoforms reported to date, namely Smaug1, Smaug1 ΔEIII and Smaug2 can act rather redundantly for one another.

The main function of Smaug proteins is to control mRNAs, and we investigated the effect of a Smaug1 construct – termed ΔSAM – that lacks the SAM domain and downstream region, which are required for RNA binding (Aviv et al., 2003; Green et al., 2003; Johnson and Donaldson, 2006; Oberstrass et al., 2006; Baez et al., 2011). Relevantly, ΔSAM forms cytosolic bodies in U2OS or HeLa cells (Fig. 4; Fig. S4A). We found that deletion of the domain involved in RNA binding abrogates the rescue of the phenotype (Fig. 4), strongly suggesting that mRNA regulation by Smaug1 is key to mitochondrial physiology.

Defective Smaug1 MLO condensation affects mitochondria

We aimed to investigate the relevance of Smaug1 MLO condensation. We generated Smaug1 deletion mutants with defective MLO formation, and used these tools to investigate the consequences of the lack of Smaug1 bodies on the mitochondrial network.

The domain organization of mammalian Smaug1 is depicted in Fig. 5A. Mammalian Smaug orthologs include two different protein regions termed Smaug similarity region 1 and 2 (SSR1 and SSR2), which have unknown function. Yeast SSR1 has been shown to dimerize *in vitro* (Tang et al., 2007). We conducted transient transfection experiments with the deletion constructs depicted in Fig. 5A to analyze whether they are able to form cytosolic condensates (Fig. 5B–D). Deletion of the N-terminal region including SSR1 and SSR2 abrogates Smaug1 body formation. The ΔSSR1/2 construct was always uniformly distributed in the cytosol in U2OS cells either fused to ECFP, V5 or V5-SBP (Fig. 5C,D), as well as in HeLa and Cos-7 cells (Fig. S4A). The SSR1-SSR2 fragment (SSR1/2) was not sufficient to phase-separate as it always showed a uniform distribution (Fig. 5C,D). In addition, a construct that lacked the first 53 amino acids, which includes SSR1 (ΔSSR1), was not able to form cytosolic bodies (Fig. 5A,C,D; Fig. S4A). Finally, the splicing variant ΔEIII also formed cytosolic bodies (Fig. 5C) as reported previously (Fernández-Alvarez et al., 2016).

We next evaluated the recruitment of specific Smaug1 protein regions to the bodies formed by the full-length molecule. We co-transfected specific Smaug1 regions tagged with ECFP together with full-length Smaug1 tagged with EYFP and measured the intensity of the ECFP tag inside and outside Smaug1–EYFP bodies (Fig. 5E). We found that both moieties, SSR1/2–ECFP and ΔSSR1/2–ECFP, which presented a uniform distribution when expressed alone (Fig. 5C,D), were efficiently recruited to Smaug1–EYFP bodies. In contrast, the construct termed SAM–ECFP, which includes the SAM domain and 47 amino acids downstream, behaved similarly to ECFP. Both proteins remained uniformly distributed and were not recruited to Smaug1–EYFP bodies (Fig. 5E).

In parallel, we performed pull-down assays to assess whether specific Smaug1 protein regions interact. We co-expressed the above described Smaug1 regions tagged with ECFP together with a full-length Smaug1 fused to a V5–SBP double tag. As expected, the pull-down of V5–SBP–Smaug1 efficiently recovered Smaug1–ECFP and did not significantly recover ECFP (Fig. 5F). The SSR1/2–ECFP fragment co-purified with V5–SBP–Smaug1, whereas ΔSSR1/2-ECFP was recovered less efficiently (Fig. 5F). Conversely, V5–SBP–SSR1/2 significantly co-pulled-down Smaug1–ECFP and SSR1/2–ECFP (Fig. 5F). In contrast, ΔSSR1/2–ECFP was recovered less significantly and ECFP was almost absent from the material co-pulled down with V5–SBP–SSR1/2. In all cases, a contribution of endogenous Smaug1 and Smaug2 that may bridge the transfected Smaug1 fragments together cannot be ruled out. Despite minor quantitative differences with the outcome of the imaging analysis described above (likely due to the harsher conditions of pull-down assays), taken together, these observations suggest that Smaug1 phase separation is driven by multiple protein

Journal of Cell Science (2022) 134, jcs253591. doi:10.1242/jcs.253591

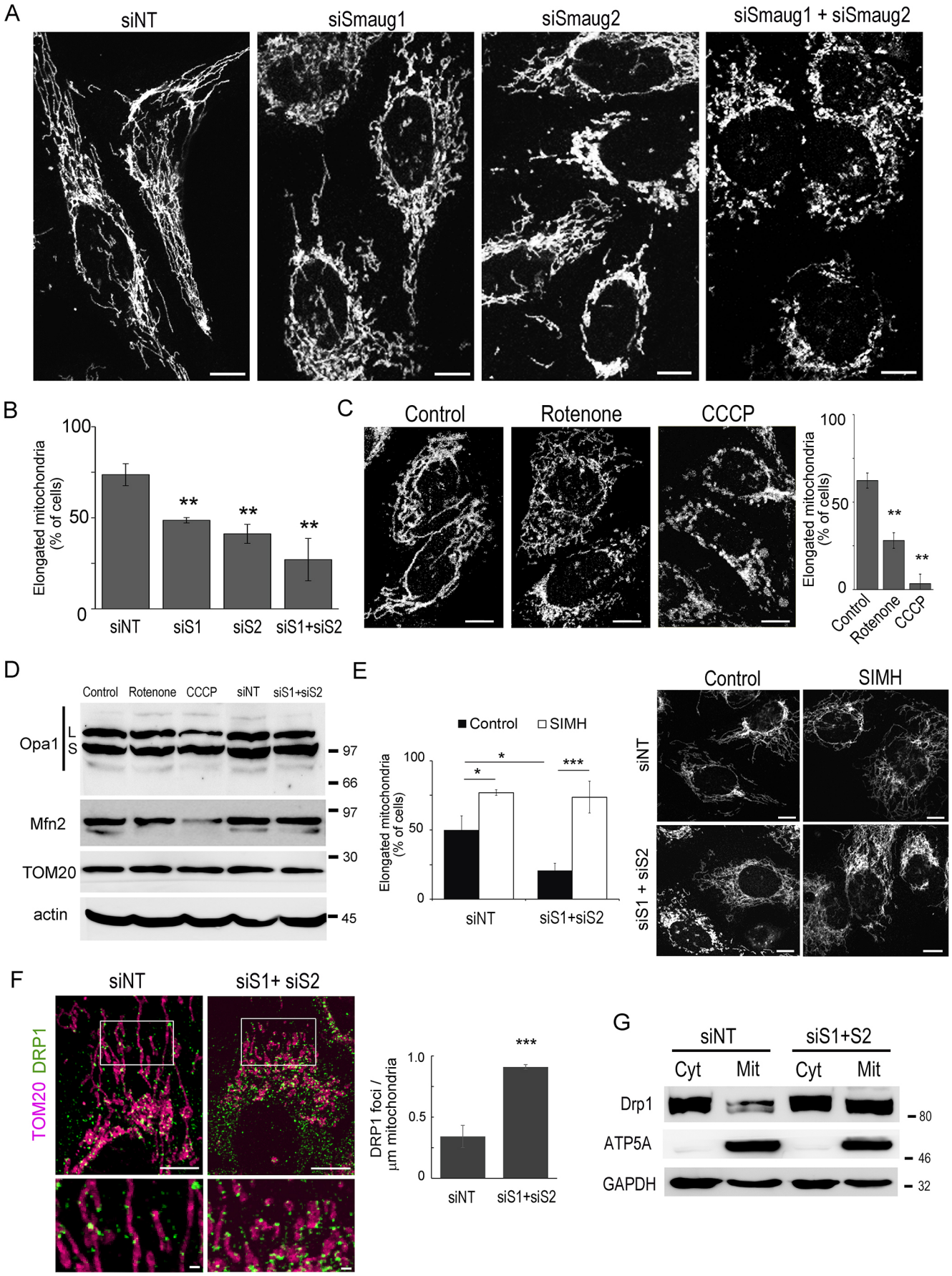

Fig. 3. See next page for legend.

Journal of Cell Science

Fig. 3. Mitochondrial network disruption upon Smaug1 and Smaug2 knockdown. (A,B) TOM20 was immunostained in U2OS cells treated with the indicated siRNAs. The percentage of cells with elongated mitochondria is plotted. Single KDs of Smaug1 and Smaug2 were analyzed in three independent experiments and the double KD was analyzed in eight independent replicates. At least 200 cells per treatment per replicate were analyzed. A representative experiment is shown. Scale bars: 10 µm. Error bars, s.d. (C) TOM20 was immunostained in U2OS cells exposed to rotenone or CCCP as indicated. At least 200 cells from duplicate coverslips were analyzed, and the percentage of cells with elongated mitochondria is plotted. A representative experiment out of three is depicted. Scale bars: 10 µm. (D) Cells were exposed to rotenone or CCCP, or either treated with the indicated siRNAs. Opa1 and Mfn2 were analyzed by western blotting. Opa1 L and S fragments are indicated. Two independent experiments were performed with similar results. (E) SIMH was induced as described in Materials and Methods and mitochondrial hyper-fusion was evaluated in at least 100 cells from duplicate coverslips for each experimental point. Means±s.d. from two independent experiments are plotted. Scale bars: 10 µm. (F) TOM20 and DRP1 were immunostained and the number of DRP1 puncta per 1 µm mitochondria was determined in 5–10 ROIs from 40 cells for each treatment. Means±s.d. from two independent experiments are plotted. Scale bars: 10 µm (whole cells), 1 µm (magnified view). (G) Western blot of DRP1 in cytosolic (Cyt) and mitochondrial (Mit) fractions. ATP5A and GAPDH were simultaneously analyzed. Two independent experiments were performed with similar results. *P<0.05; **P<0.01; ***P<0.001 (one-way ANOVA and Tukey post-test).

regions. It likely involves SSR1 homodimerization and additional interactions between yet unknown protein motifs.

We found that RNA regulation by Smaug1 affects mitochondrial function (Fig. 4), and we wondered whether condensation of Smaug1 bodies is relevant as well. We found that truncated Smaug1 constructs that show defective body formation failed to rescue the mitochondrial phenotype (Fig. 6A). Cells treated with siRNAs against Smaug1 and Smaug2 and transfected with V5-SBP-ΔSSR1/2 or V5-SBP-ΔSSR1 showed mostly short mitochondria. As above V5-SBP-ΔSAM did not rescue the phenotype whereas full-length Smaug1 rescued the mitochondrial network complexity in most cells (Fig. 6A). We conclude that mitochondrial health requires RNA binding by Smaug1 as well as the condensation of Smaug1 in specific MLOs.

Smaug1 MLO formation affects RNA binding

We next investigated the consequences of defective Smaug1 body formation on RNA regulation. To uncouple RNA binding from translational repression, we used a MS2-tethering strategy (Bhandari et al., 2014; Deng et al., 2015). Briefly, a firefly luciferase reporter carrying six MS2-binding sites (6×MS2bs) or a control reporter with no MS2-binding sites were co-transfected with the above described Smaug1 regions fused to a double tag MS2–HA. The MS2 moiety directs the tethering and the HA tag allows detection by western blotting. We found that tethering of Smaug1 reduced the expression of the 6×MS2bs reporter by ∼50% (Fig. 6B). Deletion of SSR1 and SSR2 did not affect repression of the reporter (ΔSSR1/2; Fig. 6B). As expected, tethering of the ΔSAM construct repressed the reporter and the SAM domain had no effect. For comparison, SMG7, a key factor of the non-sense mediated decay pathway (Unterholzner and Izaurralde, 2004) was analyzed in parallel and it strongly repressed the luciferase reporter (Fig. 6B). RNA levels were not affected by tethering of either full length or truncated Smaug1 constructs, whereas SMG7 induced a significant decay (51±4% relative to the MS2 control; mean±s.d.). Similar results were observed in HEK293T (Fig. 6B) and U2OS cells, where Smaug1–MS2–HA repressed the reporter to 55±5%; ΔSSR1–MS2–HA, to 57±10% and ΔSSR1/2–MS2–HA, to 48±6%, whereas tethering of the SAM domain elicited no effect.

Theoretically, the six MS2-binding sites present in the firefly luciferase reporter could tether up to six protein molecules, and we considered whether this may drive the phase separation of the otherwise ‘soluble’ Smaug1 deletion constructs. Confocal microscopy indicated that less than 10% of the cells co-transfected with ΔSSR1/2–MS2–HA and the 6×MS2bs reporter showed HA-positive puncta (always less than five puncta per cell), whereas as expected more than 50% of the cells co-transfected with Smaug1–MS2–HA and the 6×MS2bs reporter showed numerous Smaug1–MS2–HA bodies (Fig. S4B). The presence of nanoscale condensates cannot be ruled out. Collectively, these observations indicate that the formation of Smaug1 bodies does not significantly affect mRNA repression when Smaug1 is strongly tethered to multiple sites in the target transcript.

Next, we investigated whether Smaug1 phase separation affects the interaction with endogenous mRNAs. We analyzed SDHB and UQCRC1 mRNAs, which associate with Smaug1 MLOs and co-purify with Smaug1 (Fig. 1D–F). As expected, whereas SDHB and UQCRC1 mRNAs showed a three-fold enrichment in the Smaug1 pull-down, the ΔSAM construct failed to bind to these transcripts (Fig. 6C). Relevantly, we found that deletion of either SSR1 or both SSR1 and SSR2 moderately impaired the recovery of SDHB and UQCRC1 mRNAs. The pull-down of the condensation-defective V5–SBP–ΔSSR1 or V5–SBP–ΔSSR1/2 (Fig. 5C) recovered 60–75% of the amount of mRNA that co-purified with the full-length construct (Fig. 6C; Fig. S4C). Total levels of SDHB and UQCRC1 mRNAs were not affected by these constructs (Fig. S4D). These results indicate that the formation of Smaug1 bodies helps but it is not strictly required for the interaction of Smaug1 with its target mRNAs.

Mitochondrial respiration and the AMPK–mTOR pathway regulate Smaug1 body condensation

Collectively, the above observations suggest that the condensation of Smaug1 bodies contributes to the regulation of mRNAs relevant to mitochondrial function. We further speculated that Smaug1 bodies may respond to changes in the mitochondrial activity, which we interfered with by pharmacological approaches. We found that Complex I inhibition by exposure to rotenone during 1 h induced the dissolution of the Smaug1 bodies. On average, the number of cells with Smaug1 bodies dropped to two-thirds of the basal values (Fig. 7A). Smaug1–EYFP bodies were similarly affected and the proportion of cells with Smaug1–EYFP bodies dropped from 55% to 32%. In contrast, strong depolarization by CCCP elicited no effect on Smaug1–EYFP bodies (Fig. 7B,C).

Next, we investigated the effect of metformin, a drug widely used in the clinics that regulates energy metabolism mainly through complex I inhibition and AMPK activation (Hawley et al., 2002; Wheaton et al., 2014). We found that Smaug1–EYFP bodies responded to metformin in a dose-dependent manner (Fig. S4E) and the number of cells with Smaug1–EYFP bodies significantly decreased after a 1 h exposure to 100 µM metformin (Fig. 7B,C). Endogenous Smaug1 bodies similarly responded to metformin and, in accordance with previous observations (Izzo et al., 2017; Wang et al., 2017), metformin elicited no effect on the mitochondrial network (Fig. 7A). In addition, we analyzed the effect of arsenite, a known inductor of SGs, which were detected by eIF3B immunostaining (Thomas et al., 2005) (Fig. 7C). Arsenite strongly triggered SG formation and did not affect Smaug1–EYFP bodies (Fig. 7C). Rotenone and metformin did not induce SGs, and

Journal of Cell Science (2022) 134, jcs253591. doi:10.1242/jcs.253591

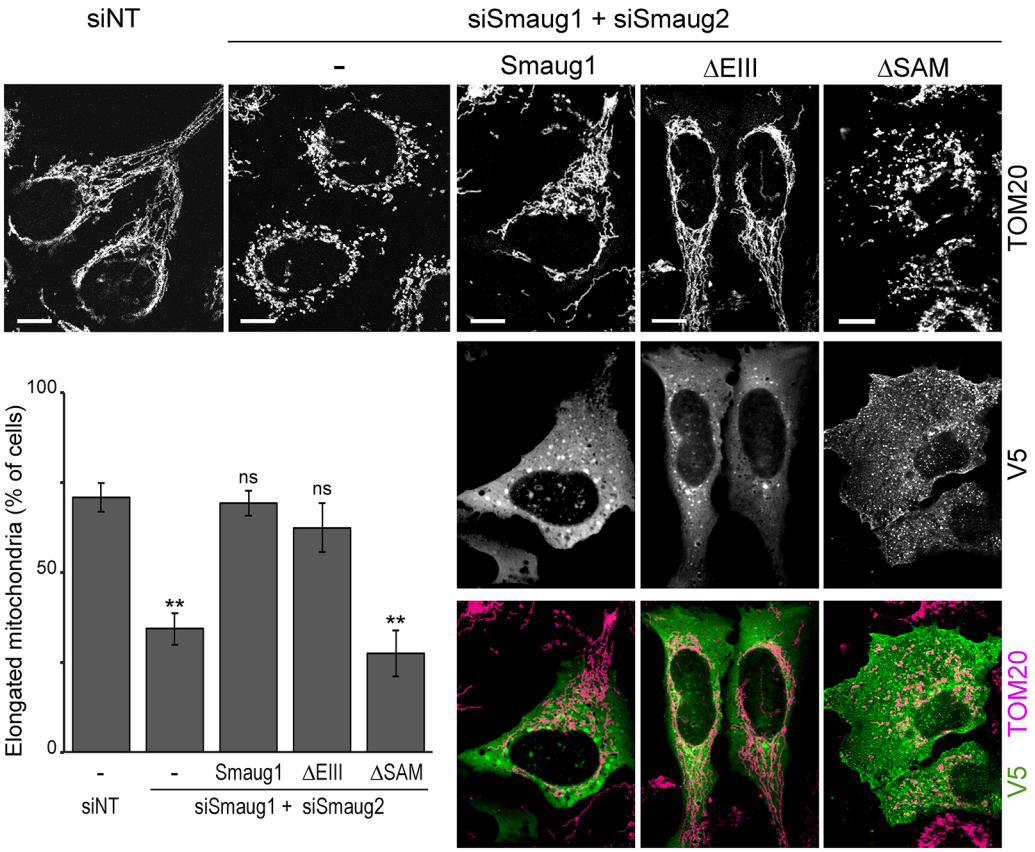

Fig. 4. Smaug binding to RNA affects mitochondria. Cells co-transfected with the indicated siRNAs and Smaug1, Smaug1 ΔEIII or Smaug1-ΔSAM tagged with V5-SBP were immunostained for TOM20 and V5. The percentage of cells with elongated mitochondria was determined in at least 200 cells from duplicate coverslips for each condition. A representative experiment out of three is shown. Scale bars, 10 µm. Error bars, s.d. ***P*<0.01; ns, not significant (one-way ANOVA and Tukey post-test).

CCCP did so moderately, as previously described (Kedersha et al., 2002). These observations indicate that the disappearance of Smaug1 body does not correlate with cellular or mitochondrial damage but rather with complex I inhibition. Mitochondrial function and cellular energetics affect the AMPK and mTOR pathways, which act antagonistically. We investigated the effect of rapamycin, a known mTOR inhibitor. We found that exposure to rapamycin triggered Smaug1–EYFP body dissolution to a similar extent to that of metformin or rotenone (Fig. 7B,D). Finally, we assessed the effect of Compound C, an AMPK inhibitor (Zhou et al., 2001). We found that Compound C completely abrogated the dissolution of Smaug1–EYFP bodies triggered by metformin, rotenone or rapamycin (Fig. 7D). Altogether, these observations collectively suggest that complex I inhibition and the subsequent AMPK activation and mTOR inhibition govern Smaug1 body dissolution.

Although unlikely, we considered whether the dissolution of Smaug1 bodies triggered by these stimuli is the consequence of a global translation activation, as proposed for SGs in other cellular contexts. We analyzed the effect of rotenone, CCCP, metformin and rapamycin in translation, which was measured by means of puromycin incorporation as previously described (Enam et al., 2020). As expected, rotenone and CCCP reduced translation, whereas metformin elicited a moderated effect and rapamycin did not induce significant changes (Fig. 7E), as reported previously (Fessler et al., 2020; Larsson et al., 2012). These observations indicated that Smaug1 body dissolution does not correlate with increased global translation. By contrast, Smaug1 body dissolution occured simultaneously with a global decrease in translation upon exposure to rotenone.

Next, we performed time-lapse confocal microscopy of Smaug1–EYFP-transfected cells exposed to metformin. We found that the response is fast. As observed in fixed cells (Fig. 7B), about half of the cells responded to metformin, and Smaug1–EYFP bodies started to dissolve immediately after treatment (Fig. 8A,B; Movies 2, 3). Smaug1–EYFP bodies showed a gradual reduction in size and/or fluorescence intensity and a significant proportion of bodies completely vanished (Fig. 8A magnified views, 8B; Movies 2, 3).

We have previously reported that the dissolution of Smaug1 bodies upon synaptic stimulation correlates with the release and translational activation of specific mRNAs (Baez et al., 2011; Luchelli et al., 2015). We speculated that the dissolution of Smaug1 bodies upon exposure to metformin is similarly linked to mRNA release. We performed co-pulldown assays as in Fig. 1, and found that metformin reduced the amount of SDHB and UQCRC1 mRNAs that co-pulled down with V5–SBP–Smaug1, whereas their total levels remained unchanged (Fig. 8C; Fig. S4F,G). We speculated that Smaug1 body dissolution correlates with the translational activation of bound mRNAs. We analyzed the effect of translational inhibitors that either enhance or halt polysome assembly, as previously undertaken (Baez et al., 2011; Buchan and Parker, 2009). We found that puromycin, which disrupts polysomes, completely abrogated the dissolution of Smaug1–EYFP bodies triggered by either rotenone, metformin or rapamycin treatment (Fig. 8D). Collectively, these observations suggest that rotenone,

Journal of Cell Science (2022) 134, jcs253591. doi:10.1242/jcs.253591

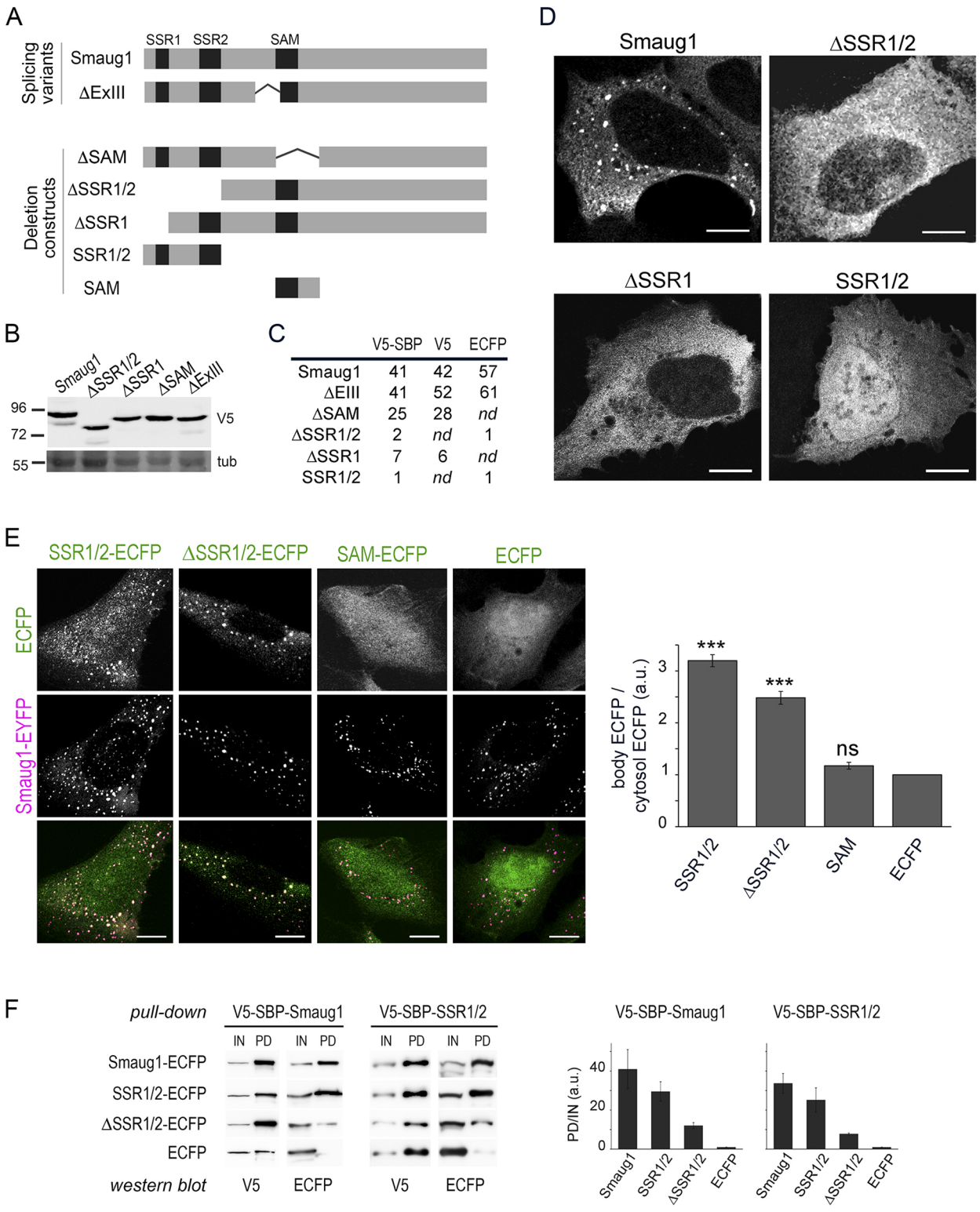

Fig. 5. A conserved region is required for Smaug1 body formation. (A) Human Smaug1 splicing variants and deletion constructs analyzed in this work. (B) Western blot of U2OS cells transfected with the indicated constructs tagged with V5-SBP. (C) The indicated constructs tagged with either V5-SBP, V5 or ECFP were transfected and the percentage of cells with cytosolic puncta was assessed by confocal microscopy. At least 200 cells from duplicate coverslips were analyzed in each replicate. Between two and six independent transfections were performed for each construct. (D) Representative images of cells expressing the indicated constructs tagged with V5–SBP. (E) Recruitment of Smaug1 protein regions to Smaug1–EYFP bodies. U2OS cells were co-transfected with Smaug1–EYFP and the indicated constructs tagged with ECFP. The ECFP signal intensity in the Smaug1–EYFP bodies relative to the cytosolic ECFP signal was measured for more than 150 Smaug1 bodies from randomly selected cells and averaged values are plotted. A representative experiment out of two is depicted. (F) V5–SBP–Smaug1 or V5–SBP–SSR1/2 were co-transfected with ECFP, Smaug1-ECFP, SSR1/2-ECFP or ΔSSR1/2-ECFP. Pull-down was performed as indicated and the presence of V5- and ECFP-tagged constructs in cell lysates (IN) or pulled-down material (PD) was analyzed by western blotting. A representative experiment out of three is shown. The ECFP signal in the PD normalized to ECFP signal in the lysate is plotted for each construct. Scale bars: 10 µm. Error bars, s.d. ***P<0.001; ns, not significant (one-way ANOVA and Tukey post-test).

Journal of Cell Science

Journal of Cell Science (2022) 134, jcs253591. doi:10.1242/jcs.253591

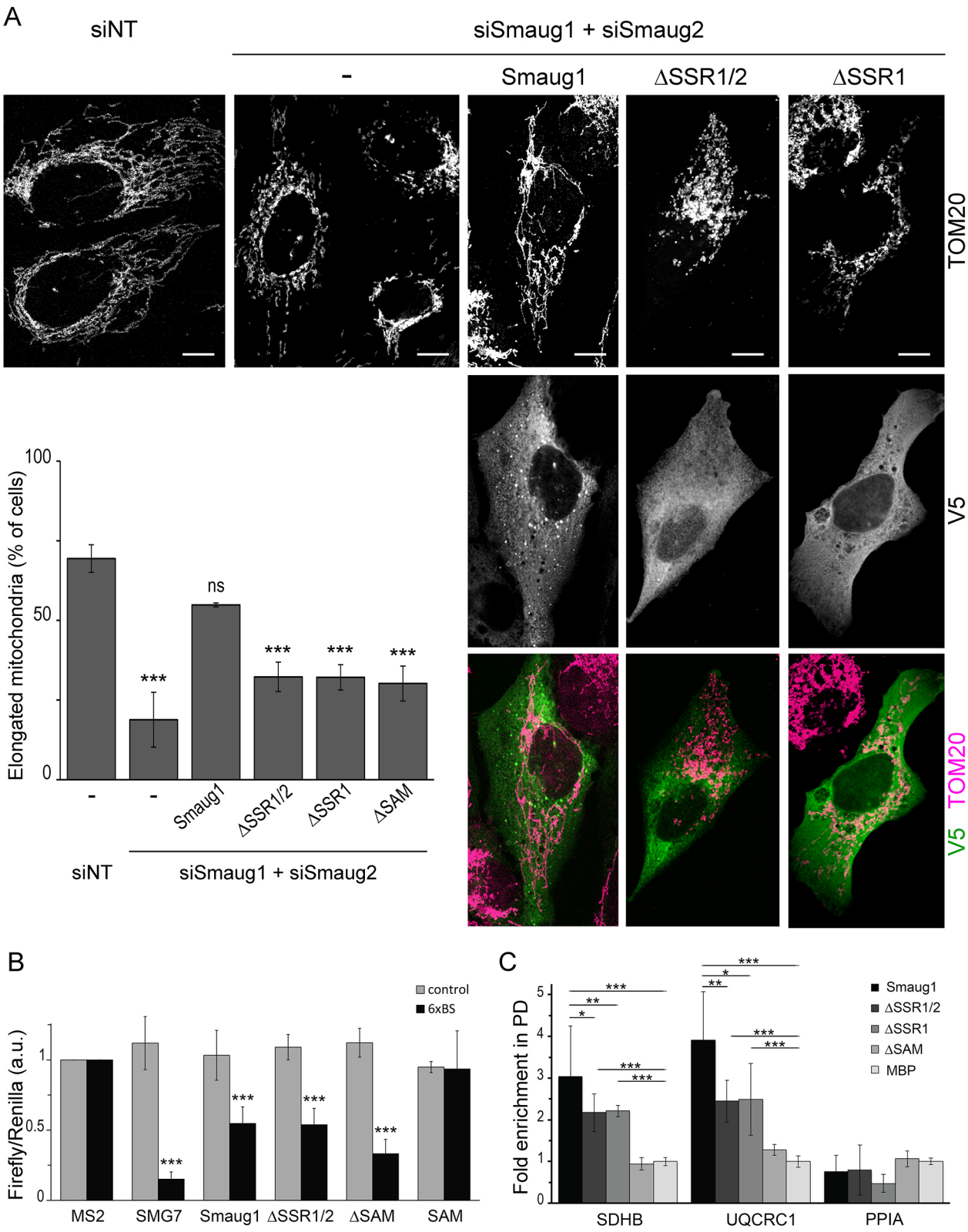

Fig. 6. Defective Smaug1 body formation correlates with mitochondrial defects. (A) U2OS cells were co-transfected with the indicated siRNAs and constructs tagged with V5–SBP. The mitochondrial network was analyzed by TOM20 immunostaining in at least 200 cells from duplicate coverslips. A representative experiment out of three is shown. Scale bars: 10 µm. (B) Tethering assay of the indicated Smaug1 constructs tagged with MS2-HA. Two firefly reporters – with or without a tandem array of 6 MS2 binding sites (6xBS) – were analyzed in parallel and normalized to a co-transfected *Renilla* reporter. The firefly/renilla ratio averaged from six independent experiments is plotted. (C) RNA pull-down. The indicated constructs tagged with V5-SBP were pulled-down and the recovery of the indicated mRNAs was determined by RT-qPCR as in Fig. 1. Average fold enrichment from five independent experiments is plotted. Error bars, s.d. **P*<0.05; ***P*<0.01; ****P*<0.001; ns, not significant (one-way ANOVA and Tukey post-test).

Journal of Cell Science (2022) 134, jcs253591. doi:10.1242/jcs.253591

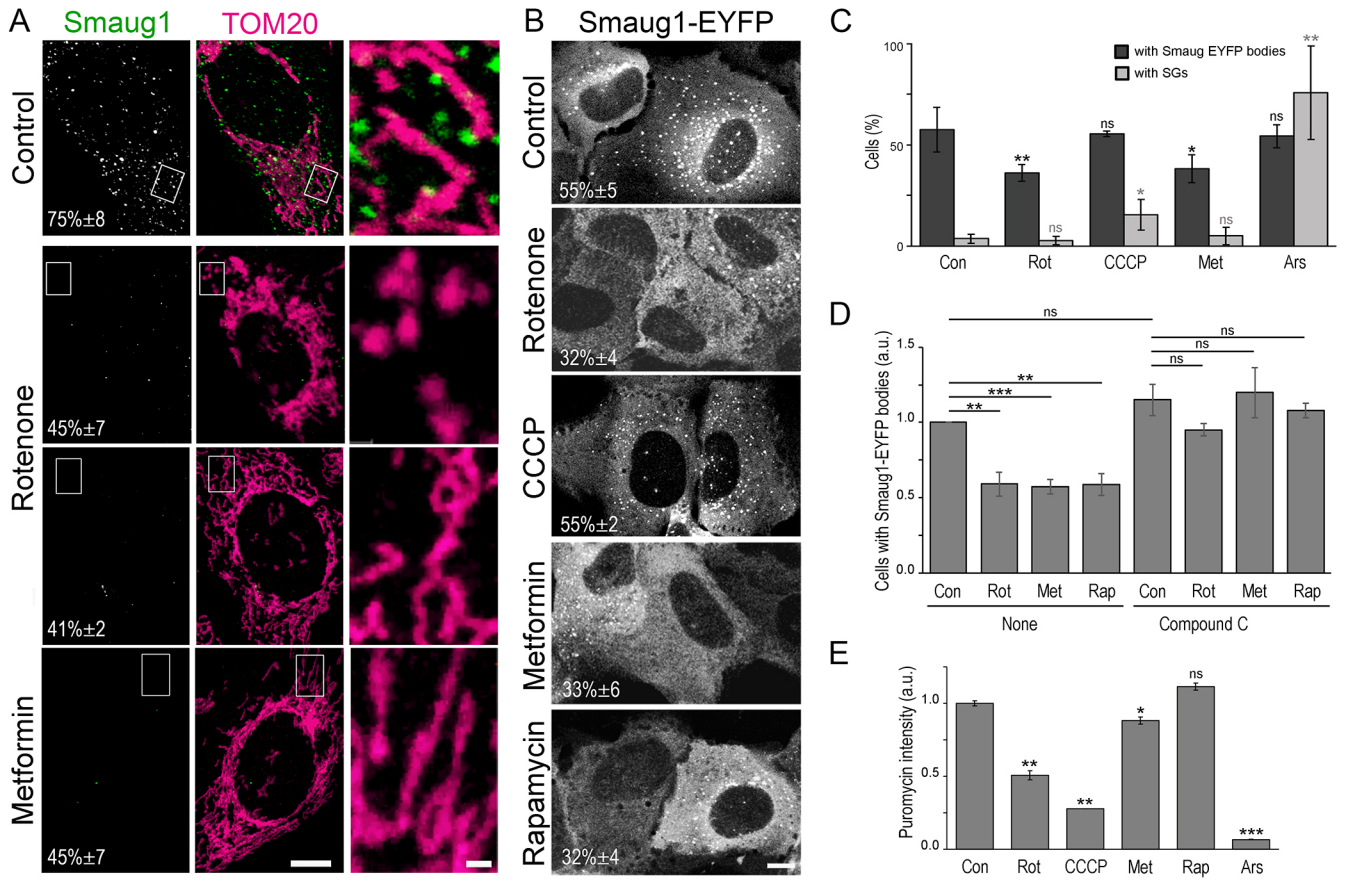

Fig. 7. Rotenone, metformin and rapamycin induce Smaug1 body dissolution. (A) U2OS cells were exposed to 2 µg/ml rotenone or 100 µM metformin during 1 h and stained for Smaug1 (green) and TOM20 (magenta). The presence of Smaug1 bodies was evaluated in at least 200 cells from duplicate coverslips for each condition and average values±s.d. are indicated. Three independent experiments were performed. Representative cells showing Smaug1 body disappearance are shown. Scale bars: 10 µm (whole cells), 1 µm (magnified views). (B) Cells transfected with Smaug1–EYFP were exposed to rotenone, CCCP, metformin or rapamycin and analyzed by confocal microscopy. Three independent experiments were performed. A minimum of 200 cells in duplicate coverslips were analyzed and mean±s.d. values corresponding to a representative experiment are indicated. Scale bar: 10 µm. (C) Cells transfected with Smaug1–EYFP were treated for 1 hour with rotenone, CCCP or metformin as above, or with 0.25 mM arsenite, and the presence of Smaug1-EYFP bodies and SGs was analyzed. More than 200 cells in duplicate coverslips were analyzed for each experimental point. A representative experiment out of two is shown. Error bars, s.d. (D) Cells transfected with Smaug1–EYFP were treated with rotenone, CCCP, metformin or rapamycin with or without simultaneous exposure to 10 µM Compound C. The presence of Smaug1–EYFP bodies was analyzed in more than 200 cells from duplicate coverslips. Three independent experiments were performed and average values are indicated. Error bars, s.d. (E) Cells were exposed to rotenone, CCCP, metformin or rapamycin as above and labeled with puromycin during 5 min as described in the Materials and Methods. At least 80 cells from duplicate coverslips for each experimental point were analyzed. Average values from two independent experiments are plotted. *P<0.05; **P<0.01; ***P<0.001; ns, not significant (one-way ANOVA and Tukey post-test).

metformin and rapamycin trigger the dissolution of Smaug1 MLOs and the release of bound mRNAs, thus enabling their translation.

DISCUSSION

Here, we report that Smaug1 MLOs contain SDHB and UQCRC1 mRNAs and that defective Smaug1 MLO condensation correlates with altered mitochondrial function. In addition, the inhibition of mitochondrial respiration, which is followed by AMPK stimulation and mTOR inactivation, rapidly triggers Smaug1 MLO dissolution and mRNA release. We hypothesize that dynamic Smaug1 MLO formation links mitochondrial function with the regulation of mRNAs that encode mitochondrial enzymes (Fig. 8E).

As reported before in neurons, the Smaug1 bodies present in U2OS cells lack ribosomes and dissolve when mRNAs are trapped into polysomes, as illustrated by the effect of cycloheximide. These observations strongly suggest that Smaug1 bodies contain repressed mRNAs that can be released to enter translation. Importantly, Smaug1 bodies are different from PBs, which similarly respond to cycloheximide and have been proposed to coordinate the expression of specific sets of functionally related mRNAs that are termed ‘RNA regulons’ (Hubstenberger et al., 2017). Relevantly, *Drosophila* Smaug binds several transcripts that code for mitochondrial proteins. Among others, mRNAs encoding ETC components, mitochondrial ribosomal proteins and additional factors involved in mitochondrial translation and protein import were reported to co-immunoprecipitate with *Drosophila* Smaug, thus likely defining a mitochondrial regulon connected to Smaug bodies (Table S1) (Chartier et al., 2015; Chen et al., 2014a; Schatton and Rugarli, 2018; Tadros et al., 2007). The collective dysregulation of all these mRNAs might contribute to the phenotype provoked by the loss of function of mammalian Smaug proteins, characterized by altered OXPHOS and a disrupted mitochondrial network.

Smaug bodies are highly motile and undergo sporadic fusion, which is characteristic of MLOs. Current models for MLO formation propose that multiple contacts involving RNA and protein molecules direct a LLPS process, which eventually drive condensation (Courchaine et al., 2016; Guo and Shorter, 2015; Perez-Pepe et al., 2018; Sachdev et al., 2019; Van Treeck et al.,

Journal of Cell Science (2022) 134, jcs253591. doi:10.1242/jcs.253591

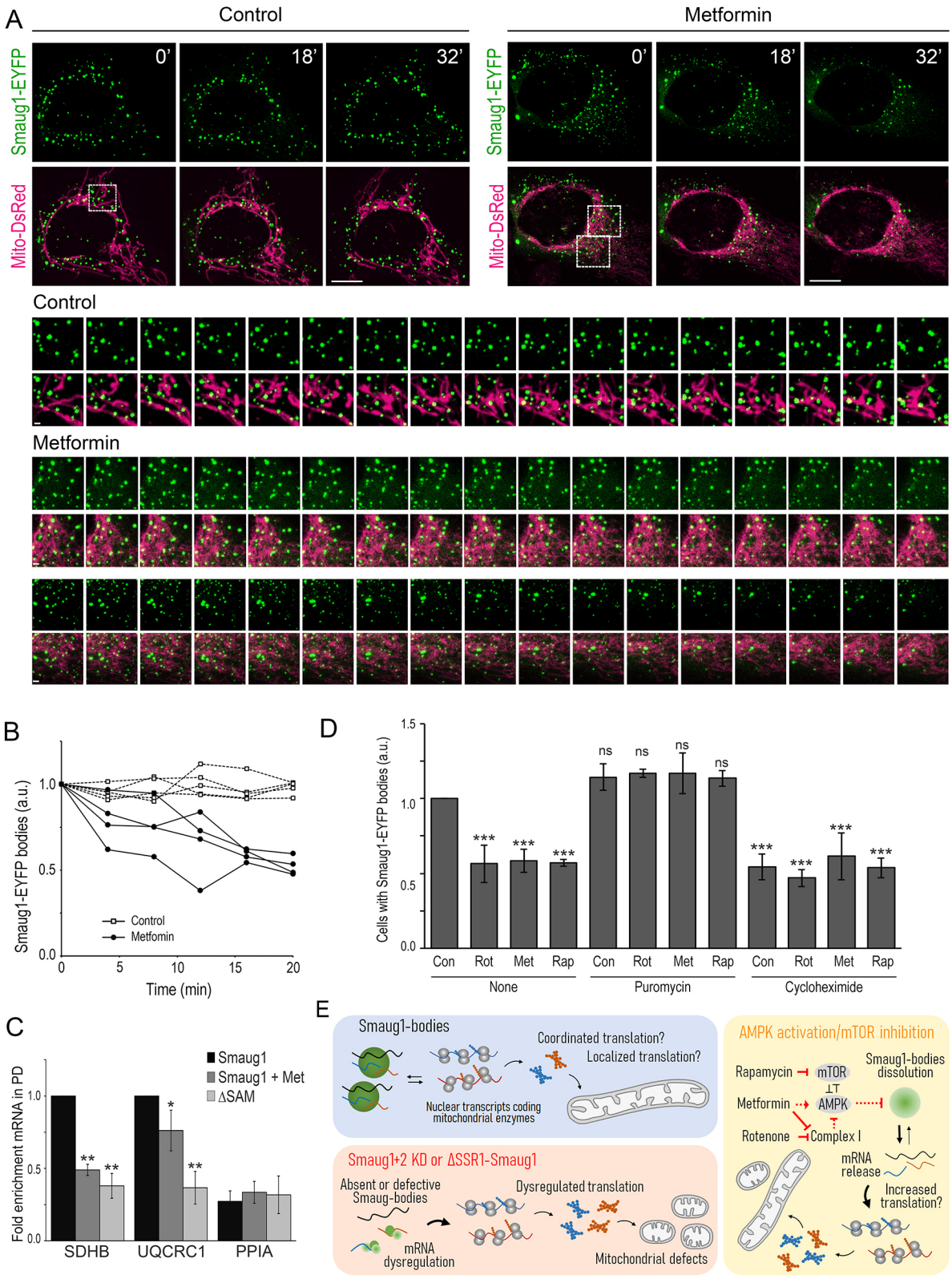

Fig. 8. See next page for legend.

2018). Here, we identified conserved Smaug1 regions involved in Smaug1 LLPS. We propose that dimerization of SSR1 domains and additional intermolecular interactions, including binding to RNA, direct the phase separation of Smaug1. The role of Smaug1 partners in Smaug1 de-mixing remains unknown (Amadei et al., 2015a; Chartier et al., 2015; Nelson et al., 2004; Pinder and Smibert, 2013). Relevantly, we found that Smaug1 condensation does not influence translation repression per se. However, truncations that affect Smaug1 MLO condensation reduce the interaction with target mRNAs. We speculate that the presence of multiple RNA-binding

Journal of Cell Science

Fig. 8. Pharmacological inhibition of AMPK impairs Smaug1 body dissolution. (A,B) Live-cell imaging of U2OS cells transfected with Smaug1–EYFP and Mito-DsRed and exposed to 100 µM metformin. Representative control and metformin-treated cells at 0, 18, and 32 min are shown. Magnifications of the indicated areas at 2-min intervals are shown from 0 to 32 min. Scale bars: 10 µm (whole cells), 1 µm (magnified views). (B) The number of Smaug1–EYFP bodies in four control and four metformin-treated cells normalized to pre-treatment values is plotted. Three independent experiments were performed with similar results. (C) U2OS cells transfected with V5–SBP–Smaug1 were exposed to metformin and the levels of co-pulldown of SDHB, UQCRC1 and PPIA mRNAs was determined by RT-qPCR. The pull-down/input ratio normalized to RpLp0 mRNA values are plotted for each transcript. Cells transfected with V5-SBP-ΔSAM were analyzed in parallel. Average fold-enrichment from three independent experiments is plotted. Error bars, s.d. (D) Cells transfected with Smaug1–EYFP were exposed to rotenone, metformin or rapamycin as above with or without simultaneous exposure to puromycin or cycloheximide. More than 200 cells from duplicate coverslips were analyzed for each experimental point. Average values from two independent experiments are plotted. Error bars, s.d. **P*<0.05; ***P*<0.01; ****P*<0.001; ns, not significant (one-way ANOVA and Tukey post-test). (E) Summary and proposed model. Smaug1 forms dynamic MLOs that contain mRNAs for mitochondrial proteins, such as SDHB and UQCRC1 mRNAs, and may affect their expression at several levels, including localization or coordinated translation. The absence or the defective formation of Smaug1 and Smaug2 bodies affect mitochondrial function as a consequence of the dysregulation of specific mRNAs. Exposure to the antidiabetic drug metformin as well as complex I inhibition with rotenone, or mTOR inhibition with rapamycin trigger the dissolution of Smaug1 bodies involving AMPK activation. A direct effect of AMPK on Smaug1 remains to be investigated. Smaug1 body dissolution enables the release of mRNAs coding for mitochondrial enzymes and likely other cellular functions, thus contributing to regulate the energetic balance.

domains in Smaug1 bodies will increase the avidity for mRNA molecules, as similarly proposed for yeast Vts1 (Bieman, 2014).

We found that defective Smaug1 body condensation seriously affects mitochondria, likely as a consequence of concurrent mechanisms that remain to be further investigated. A single Smaug1 body can contain several mRNA species, as shown here for UQCRC1 and SDHB mRNAs. Additional transcripts are likely to be present simultaneously; this might enable their coordinated regulation, speculatively facilitating the biogenesis of multimolecular protein complexes. The importance of the co-translational assembly of mitochondrial complexes is illustrated by the serious defects linked to mutations in SDH assembly factors. In addition, several nuclear messengers that encode mitochondrial proteins including complex I and II subunits have been shown to be translated at the mitochondria periphery in yeast, plant and animal cells (reviewed in Moosavi et al., 2019; and see Gehrke et al., 2015; Schatton and Rugarli, 2018; St-Pierre and Topisirovic, 2016; Vincent et al., 2017; Wilk et al., 2016; Williams et al., 2014; Wu et al., 2018). The sporadic contact of Smaug1 MLOs with mitochondria may be linked to the local regulation of specific mRNAs or to the coordination of their translation (Fig. 8E). A parallel between Smaug1 MLOs and the MLOs formed by the RNA binder Tis11, which associates to the endoplasmic reticulum (ER), thus affecting ER-associated translation, seems attractive (Béthune et al., 2019; Kuzniewska et al., 2020; Ma and Mayr, 2018).

The translation of mitochondrial enzymes responds to the mitochondrial physiology and cellular energetics (Béthune et al., 2019; Gao et al., 2014; Schatton et al., 2017; Wakim et al., 2017; Wu et al., 2018). Relevantly, along with the significance of Smaug1 body formation to mitochondrial function, we found that acute complex I inhibition and changes in the AMPK–mTOR balance trigger Smaug1 body dissolution. We have recently shown that *Drosophila* Smaug MLOs are affected by Smoothened (Smo), a key molecule in the Hedgehog (HH) pathway (Bruzzone et al., 2020). Whether Smaug regulation by Smo is conserved in mammals and whether this occurs in connection with changes in mitochondrial activity is currently unknown.

The release of mRNAs from dissolving MLOs is linked to their translation activation (Baez et al., 2011; Khong and Parker, 2018; Moon et al., 2019) and thus, we speculate that Smaug1 body dissolution enables the translation of SDHB, UQCRC1 and other transcripts directly involved in mitochondrial function. The role of Smaug orthologs as post-transcriptional regulators of energetic metabolism appears to be evolutionarily conserved as yeast Vts1p, which forms MLOs and prion-like condensates, controls mRNAs linked to nutrient sensing (Chakravarty et al., 2020; She et al., 2017). Smaug1 MLOs emerge as important regulatory hubs that respond to changes in mitochondrial respiration and AMPK stimulation, thus activating the translation of specific transcripts. Relevantly, complex I inhibition by metformin was shown to repress the translation of a number of mRNAs (Howell et al., 2017; Kalender et al., 2010; Larsson et al., 2012; Morita et al., 2013), and we propose that Smaug1 MLOs add a new pathway for translational reprogramming downstream of AMPK–mTOR.

A reduced number of RNA-binding proteins, including the highly conserved factors Pumilio and clustered mitochondria homolog (CLUH), are involved in the regulation of nuclear-encoded transcripts that encode mitochondrial proteins (reviewed in D'Amico et al., 2019; Gao et al., 2014; Gehrke et al., 2015; Kopp et al., 2019; Lee and Tu, 2015; Olivas and Parker, 2000; Pla-Martín et al., 2020; Schatton et al., 2017; Schatton and Rugarli, 2018; Vardi-Oknin and Arava, 2019; Wakim et al., 2017). The putative interplay between these regulatory pathways and Smaug remains to be investigated.

Besides its relevance to cancer and diabetes, mitochondrial activity is particularly important in normal tissues with high energy demands, including neurons and muscle cells. Mitochondrial defects are causative of several neurological conditions and muscular dystrophies (Friedman and Nunnari, 2014; Gan et al., 2018; Kriaucionis et al., 2006; Rangaraju et al., 2019; Rugarli and Langer, 2012; Shan et al., 2019). The strong effect of Smaug1 and Smaug2 in neuronal and muscular cells is likely related to the relevance of Smaug to mitochondrial function (Amadei et al., 2015b; Baez et al., 2011; Chartier et al., 2015; Chen et al., 2014b; de Haro et al., 2013; Luchelli et al., 2015; Thomas et al., 2014). The present work opens new questions on the motility and dynamics of Smaug bodies in a wide diversity of cellular contexts. A major issue to be addressed is how these MLOs respond to metabolic cues and what are the consequences for the transport and translation of mRNAs that encode mitochondrial enzymes.

MATERIALS AND METHODS

Cell culture and treatments

U2OS and HEK293T cells were obtained from the American Tissue Culture Collection (ATCC) and grown and maintained as indicated. Cell lines were transfected with Jet Prime (Polyplus Transfection) according to the manufacturer's instructions.

pCDNA6-V5-hSmaug1 (Smaug1-V5) and pECFP-N1-hSmaug1 (Smaug1-ECFP) constructs were previously described (Baez and Boccaccio, 2005). Smaug1-EYFP was prepared by direct sub-cloning of pECFP-N1-hSmaug1 into pEYFP-N1 (Clontech). ΔSAM-hSmaug1-ECFP and ΔSAM-hSmaug1-EYFP with a deletion of amino acids 318 to 424 were constructed by splicing by overlap extension (SOE)-PCR using ECFP-ΔC-hSmaug1 and hSmaug1-ECFP as templates and the following primers (SOE-1, 5′-GCGAGCCTCGGGTGTGTTACGAGC-3′; SOE-2, 5′-GCTCGTAACACACCCGAGGCTCGC-3′). ΔSAM–hSmaug1–V5 was

obtained by insertion into pcDNA6.0-B-His-V5 (Clontech) using HindIII/XhoI restriction digestion. ECFP–ΔC-hSmaug1, which comprises amino acids 2 to 418 was constructed by PCR using T7 5′-TAATACGACTCACTATAGGG-3′ forward and 5′-AAGGCGAGCCTCGAGGGTG-3′ reverse primers and pCDNA6-V5-hSmaug1 as template with XhoI/HindIII deletion fragment inserted in a SalI/HindIII pECFP-C3 digested vector (Clontech). ΔSSR1-hSmaug-V5 spans amino acids 54 to 718 and was constructed by PCR using forward primer 5′-GCTCCCAAGCTTACCATGGAGCTGCACGTCCTCGAACG-3′ and reverse primer 5′-GCTCCGCTCGAGAAGATGGTGGAGGTCCGGTCAAC-3′ and hSmaug1-V5 as template and pcDNA6.0-B-His-V5 as vector. SSR1/2-hSmaug1-ECFP was constructed by insertion of a HindIII/SalI fragment into pECFP-N1 and spans amino acids 2 to 154. All MS2–HA constructs were obtained by PCR using primers carrying BamHI and XhoI restriction sites and pcDNA3.1-MS2-HA (Lykke-Andersen et al., 2000). V5-SBP-hSmaug1 was cloned by PCR using primers carrying XhoI and BamHI sites into pT7-V5-SBP (Sgromo et al., 2017). V5-SBP-ΔSAM-hSmaug1 was sub-cloned by KpnI/BamHI restriction of ΔSAM-hSmaug1-ECFP. V5-SBP-ΔN-hSmaug1 was cloned by BamHI/SacII digestion into a BglII/SacII pT7-V5-SBP-C1 digested plasmid. V5-SBP-ΔN-hSmaug1 was cloned by BamHI/EcoRI digestion into a BglII/EcoRI pT7-V5-SBP-C1 digested plasmid.

For knockdown experiments, U2OS cells were treated with 50 nM siRNAs using Jet Prime transfection reagent for 48 h following the manufacturer's instructions. siRNAs were obtained from Dharmacon or Eurofins and were: non-targeting (NT), 5′-UAGCGACUAAACACAUCAA-3′; Samd4A mix, (1) 5′-GACCAGAGGGUUUGCGAA-3′, (2) 5′-CUACAGGUAUAUAGCUCAA-3′, (3) 5′-CUUAAUGAAAUCCGAACAA-3′ and (4) 5′-GAUGGAAAUGACAGCGCUA-3′; Samd4B mix, or sequences 1 or 4 alone, (1) 5′-ACACAGAGGCCAAGUCGGA-3′, (2) 5′-CAUGAGGCUUUCACGGAGA-3′, (3) 5′-AUCCAGAAGCUGCGUGAGA-3′ and (4) 5′-GCUGAAGCUCCUCCGGACA-3′.

Drug treatments were as follows: metformin hydrochloride (Sigma-Aldrich) was dissolved in H_2O and used for 1 h at 500 µM, unless otherwise indicated. Rotenone was used at 2 µg/ml (from a 50 mg/ml stock solution in DMSO) for 1 h unless otherwise indicated. Carbonyl cyanide m-chlorophenyl hydrazine (CCCP) was used at 20 µM (from a 100 mM stock solution in DMSO) for 1 h unless otherwise indicated. Ramapycin (LC-Laboratories) was used at 50 nM (from a 4 mM stock solution in DMSO) for 1 h, unless otherwise indicated. Compound C (Sigma-Aldrich) was used for 1 h at 10 µM (from a 10 mM stock solution in DMSO), unless otherwise indicated. To induce SIMH, cells were exposed to 1 µM cycloheximide for 3 h (Ehses et al., 2009; Tondera et al., 2009). Sodium arsenite (Sigma-Aldrich) was used at 1 mM, and cycloheximide and puromycin (Sigma-Aldrich) were used at 250 µg/ml, all for 1 h, unless otherwise indicated.

Immunofluorescence, FISH and puromycilation

Immunofluorescence of cultured cells was performed after fixation, permeabilization and blocking as usual (Baez et al., 2011; Fernández-Alvarez et al., 2016; Luchelli et al., 2015). Primary antibodies were diluted as follows: V5 (46-0705, Invitrogen), 1:500; anti-SAMD4A (HPA043061, Sigma), 1:20; anti-ubiquitin Ubi-1 (ab7254, abcam), 1:500; anti-DRP1 (EPR19274, abcam), 1:250; anti-TOM20 (sc-17764, Santa Cruz Biotechnology), 1:200; anti-UQCRC1 (ab110252, abcam), 1:50; anti eIF3n (sc-16377, Santa Cruz Biotechnology), 1:200.

Secondary antibodies coupled to Alexa Fluor 488 (Invitrogen) or Cy3 (Jackson Immuno Research Laboratories, Inc.) were used at 1:300–1:500. For MitoTracker™ Red CMXRos (Invitrogen) staining, cells were incubated for 45 min at 37°C with 400 nM MitoTracker and washed three times with conditioned medium prior to 4% paraformaldehyde (PFA) fixation.

FISH for ribosomal RNA was performed using digoxigenin-labeled riboprobes as previously described (Thomas et al., 2005). Single-molecule FISH with Stellaris probes (Biosearch Technologies) was performed according to manufacturer's instructions.

Labeling of translating polypeptides was performed by incubating the cells in complete medium with 10 nM puromycin (Sigma) for 10 min, followed by fixation and detection with anti-puromycin (1:25, PMY-2A4, DSHB) and Alexa Fluor 488-conjugated secondary antibody. Fluorescence intensity in single cells was measured using ImageJ (https://imagej.nih.gov/ij/) and the average from 100 cells was calculated for each experimental point in duplicate coverslips.

Images were acquired with PASCAL-LSM, LSM510 Meta, or LSM 880 confocal microscopes (Carl Zeiss), using C-Apochromat 40×/1.2 W Corr or 63×/1.2 W Corr water immersion objectives for the PASCAL-LSM, an EC 'Plan-Neofluor' 40×/1.30 NA oil or Plan-Apochromat 63×/1.4 NA oil objective lenses for the LSM510 Meta, and a Plan-Apochomat 63×/1.4 Oli DIC M27 objective for the LSM880. Pixel intensity was always lower than 250 (saturation at 255). Cell contours in Fig. 1B,E were manually drawn using saturated immunofluorescence images as templates.

Image analysis

To evaluate the presence of Smaug1 bodies or Smaug1–EYFP bodies in fixed cells, cells were manually classified as positive when more than three bodies of at least 0.25 µm in diameter were present. For single-molecule FISH confocal images, we used a previously described strategy (Luchelli et al., 2015) to evaluate the frequency of stochastic contacts of SDHB and UQCRC1 mRNAs with Smaug1–EYFP bodies. Briefly, three cognate images of the Smaug1–EYFP channel were generated by flipping and/or mirroring the original, and the presence of mRNA contacting or colocalizing with Smaug1–EYFP bodies was inspected manually and by determining a Manders' coefficient. Randomly selected cells were analyzed and between three and seven regions of intertest (ROIs) covering almost all the cytosolic area were used. To evaluate contacts with mitochondria, ROIs were selected and automatically segmented by means of a custom-made Python script (available upon request). Smaug1 bodies, mitochondria and cells were segmented by means of Laplacian of Gaussian filter to highlight round structures followed by triangle thresholding, watershed to separate clustered objects, mean thresholding and different sets of morphological operations (such as closing, erosion and dilations). Euclidean distance between the border of bodies and nearest mitochondria was calculated for each body and they were classified as 'in contact' when this distance was 0. To evaluate the statistical significance, the positions of the Smaug1 bodies were randomized ten times and distance to mitochondria was calculated in the randomized images as before (Denes et al., 2021). Experimental vs random values were analyzed by paired two-tailed *t*-test.

Confocal live-cell imaging

A Carl Zeiss LSM 880 inverted confocal microscope equipped with a stage-top heated platform maintained at 37°C and with a controlled CO_2 flux chamber was used. U2OS cells were grown and transfected in eight-well Nunc® Lab-Tek chamber slides. U2OS cells expressing hSmaug1–EYFP and Mito-DsRed were imaged 24 h after transfection. Metformin was injected into slides without opening the CO_2 chamber. *Z*-stack images were obtained for each cell every 2 min. For image analysis, acquired *z*-stacks were processed with a custom-made Python script to segment and quantify the intensity and morphological properties (Malik-Sheriff et al., 2018) of the Smaug1–EYFP bodies. The segmentation pipeline consisted of filtering the hSmaug1-EYFP channel with Laplacian or Gaussian filters and using manual thresholding to distinguish between pixels corresponding to Smaug1–EYFP bodies from background pixels. Smaug1 body pixels were later disregarded to distinguish between background and cytoplasm pixels. To analyze the effect of metformin, the number of Smaug1–EYFP bodies at each time point was normalized to the pre-treatment value for each cell. Afterwards, quantifications were binned every 4 min and averaged. For all the analysis, Python 3.7, numpy 1.15, pandas 0.23, scikit-image 0.14, and scipy 1.1 were used.

Mitochondria purification and western blotting

Whole-cell lysates were prepared by using RIPA buffer. Cytosolic and mitochondrial fractions were obtained by using the mitochondria/cytosol fractionation kit (ab65320, abcam). For AMPK and acetyl-CoA carboxylase (ACC) western blots, proteins were obtained as follows: cells were directly lysed in 1× SDS loading buffer [62.5 mM Tris-HCl (pH 6.8 at 25°C), 2% (w/v) SDS, 10% glycerol, 40 mM DTT and 0.01% (w/v) Bromophenol Blue], sonicated for 15 s in a Bioruptor® (Diagenode) at maximum intensity and heated for 5 min at 95°C. Western blotting was performed by standard

procedures using PVDF membranes (Immobilon-P, Millipore) and ECL Prime (GE Healthcare) and analyzed using a LAS4000 Imager (GE Healthcare). Primary antibodies were used as follows: anti-SAMD4A (HPA043061, Sigma), 1:100; anti-SAMD4B (HPA059385, Sigma), 1:100; mouse anti-V5 (46-0705, Invitrogen), 1:5000; anti-GFP (A11122, Invitrogen), 1:2000; anti-tubulin (DSHB), 1:10,000; anti-β-actin (A5441, Sigma-Aldrich), 1:10,000; anti-DRP1 (EPR19274, abcam), 1:1000; anti-OPA1 [EPR11057(B), abcam], 1:1000; anti-Mitofusin 2 (6A8, abcam), 1:1000; anti-TOM2O (sc-17764, Santa Cruz Biotechnology), 1:100; anti-UQCRC1 (ab110252, abcam), 1:1000; Total OXPHOS Rodent WB Antibody Cocktail (ab110413, abcam), 1:250; Phospho-AMPKα (Thr172) (40H9, Cell Signaling), 1:1000; AMPKα (D5A2, Cell Signaling), 1:1000; phospho-acetyl-coA carboxylase (Ser79) (D7D11, Cell Signaling), 1:1000, anti-acetyl coenzyme A carboxylase antibody (ab205883, abcam), 1:1000; and anti-hGAPDH (DSHB), 1:1000. HRP-conjugated secondary antibodies were used 1:10,000 or 1:100,000. Signal intensity was assessed with the ImageJ software.

Respiratory parameters and mitochondrial membrane potential

Oxygen flow in U2OS cells under ADP excess (state 3) was measured using a two-channel, high-resolution Oxygraph respirometer (Oroboros, Innsbruck, Austria), as described in Doerrier et al. (2018). Briefly, cells were treated with the indicated siRNAs for 48 h and harvested at 90% confluence in trypsin-EDTA, washed once with phosphate-buffered saline (PBS), resuspended in fresh growth medium without antibiotics at a density of 1×10^6 cells/ml, and analyzed in 2 ml Oxygraph chambers under continuous stirring at 750 rpm at 37°C in 2 s intervals. For intact cell analysis, routine respiration was recorded and then 2.5 µM oligomycin were added to inhibit ATP synthase, which allows the measurement of leak respiration. The electron transfer system (ETS) capacity was evaluated by titration with carbonyl cyanide m-chlorophenyl hydrazone (CCCP) uncoupler in 0.5 µM steps until a maximum flow was reached. Respiration was inhibited by 0.5 µM rotenone and 2.5 µM antimycin A to determine residual oxygen consumption (ROX). For digitonin-permeabilized cells, a substrate-uncoupler-inhibitor-titration protocol termed SUIT-RP2 (Doerrier et al., 2018) was performed. Oxygen flow was measured before digitonin treatment in respiration medium MiR05 (Routine), and after successive addition of substrates and inhibitors as follows: 5 mM ADP, 0.1 mM malate, 0.2 mM octanoyl-carnitine, to record the electron-transferring flavoprotein complex from fatty acid b oxidation to coQ (F pathway); 2 mM malate, 5 mM pyruvate, 10 mM glutamate to record OXPHOS in the N-junction (Gnaiger, 2020), 10 mM succinate to record the OXPHOS capacity state FNS with convergent input of electrons via complexes I and II into the respiratory system, 10 mM glycerol-3-phosphate to activate the glycerophosphate dehydrogenase shuttle; stepwise titration with CCCP in 0.5 µM increments as needed to determine the ETS capacity state at maximum oxygen flow; 0.5 µM rotenone for complex I inhibition. All respiratory coupling states were corrected for ROX, which was obtained after the addition of 2.5 µM antimycin A. Finally, 5 mM ascorbate plus 0.5 mM N,N,N′,N′-tetramethyl-p-phenylenediamine dihydrochloride (TMPD) were used as substrates to assess complex IV activity. Mitochondrial membrane integrity was verified after addition of 10 µM cytochrome *c*, and changes were always lower than 10%. Data was analyzed using DatLab7.4.0.4 software (Oroboros, Austria). Oxygen flow is expressed as picomoles per second per million cells and normalized to the mitochondrial DNA content in each sample (pmol/S×million cells×mtDNA). All experiments were performed using instrumental background correction and after calibration of the polarographic oxygen sensors. Statistical significance was calculated using Mann–Whitney rank-sum test using SPSS IBM for Windows statistical package, version 26 (SPSS Inc, Chicago, IL, USA).

Mitochondria depolarization was assessed with the MitoProbe 5′,6,6′-tetrachloro-1,1′,3,3′-tetraethylbenzimidazolylcarbocyanine iodide (JC-1; T3168, Invitrogen Molecular Probes). For cytometry assay, cells were treated with trypsin, resuspended in complete DMEM, washed twice with PBS and incubated with 2 µM JC-1 dissolved in pre-warmed PBS at 37°C, 10% CO_2 for 20 min and analyzed by flow cytometry. Exposure to 100 µM CCCP to induce complete depolarization was done for 5 min before incubation with JC-1. Flow cytometry analysis was performed using a FACS Aria (Becton Dickinson, Franklin Lakes, NJ, USA) and data mining was undertaken using FlowJo (Tree Star, Inc., Ashland, OR, USA). Fluorescence intensity of J-aggregates (red) and JC-1 monomers (green) was measured in the mCherry and FITC channels. CCCP-treated cells were used to set gates. Geometric means normalized to siNT-treated cells were calculated. Confocal live-cell imaging was performed using a Carl Zeiss LSM 880 inverted confocal microscope as described above. Cells were seeded in Lab-tek chamber slides and incubated with JC-1 and CCCP as above. Images were obtained using a 20× objective and 488/543 nm lasers, and fluorescence intensity was analyzed using ImageJ.

Pull-down assays

Cells were grown in 100 mm-plates and transfected with a mix of 250 ng of V5-SBP-tagged constructs and 250 ng of EYFP constructs. After 24 h of expression, cells were harvested with 500 µl of NET buffer (150 mM NaCl, 50 mM Tris-HCl pH 7.5, 1 mM EDTA and protease inhibitor cocktail from Sigma). Cells were kept on ice for 15 min and lysed by pipetting up and down 20 times. After a 15-min centrifugation (16,000 ***g***) to remove cell debris the supernatant (input, IN) was incubated for 1 h at 4°C with Streptavidin-conjugated beads. After three washes in NET buffer supplement with 0.1% Triton X-100 and one wash in NET buffer, pulled down proteins were cracked in protein sample buffer and subjected to western blotting for EYFP and/or V5.

RNA pull-down assays

Cells grown in 100 mm plates were transfected with 10 µg of V5–SBP-tagged constructs and harvested 24 h afterwards in 400 µl of RPD buffer (150 mM NaCl, 25 mM Tris-HCl pH 7.4, 5 mM EDTA, 0.5 mM DTT, 1% NP40, 5% glycerol and protease inhibitor cocktail from Sigma). Cells were lysed using a Bioruptor® (Diagenode) and after centrifugation (16,000 ***g***), pull-down was performed with Streptavidin-conjugated beads (17-5113-01, GE Healthcare). Total RNA from pull-down or input samples was isolated using TRIzol LS reagent (Invitrogen) following the manufacturer's instructions. First-strand cDNA was synthesized from 2 µg of total RNA using random hexamers and MMLV reverse transcriptase (Promega). The cDNA was used as a template for quantitative PCR performed using Syber Green reagent (Applied Biosystems) and the Light Cycler 480 system (Roche). The amount of the indicated mRNAs relative to RpLp0 was determined using specific primers. Binding is expressed as the relative amount of mRNA in the pull-down material normalized to the relative amount in the input sample. The levels of the tagged constructs in the inputs and pulled-down material were measured by western blotting using anti-V5 antibody. Sequences of primers were as follows: NDUFA10 Fw, 5′-AGTACTCAGATGCCTTGGAG-3′ and Rv, 5′-GCTCCAACACAACACCTTGTC-3′; UQCRC1 Fw, 5′-CCTCTCAG-CCCACTTGCA-3′ and Rv, 5′-CGGCTGCCAACATCAAT-3′; SDHB Fw, 5′-GTGGCCCCATGGTATTGGAT-3′ and Rv, 5′-CACAAGAGCCACA-GATGCCT-3′; PPIA Fw, 5′-TTCATCTGCACTGCCAAGAC-3′ and Rv, 5′-TCGAGTTGTCCACAGTCAGC-3′; RpLP0 Fw, 5′-GGGCAAGAA-CACCATGATGC-3′ and Rv, 5′-CATTCCCCCGGATATGAGGC-3′.

Tethering assays

Tethering assays were performed as previously described (Bhandari et al., 2014; Deng et al., 2015). In brief, HEK293T cells were transfected at 50% confluency with a mix of 250 ng of Smaug1-MS2-HA constructs, 200 ng of Firefly-6×MS2bs plasmid or control firefly and 50 ng of pCIneo-*Renilla* for 24 h in 24-well plates using Jet Prime reagent following the manufacturer's instructions. Luciferase expression levels were analyzed using the Dual Luciferase kit (Promega) in a DTX880 Multimode detector (Beckman Coulter).

Statistics

Each experimental point included duplicate or triplicate coverslips or wells. Cell numbers are indicated in each figure panel. Statistical significance was determined using Excel or Instat software (GraphPad Software, Inc.) in all figures unless indicated. *P*-values (**P*<0.05; ***P*<0.01; ****P*<0.001; ns,

not significant) relative to control treatments were obtained by one-way ANOVA and Tukey post-test. Error bars, represent standard deviation (s.d.) from duplicate coverslips from representative experiments or from independent experiments, as indicated. Data in Fig. 1F,G were analyzed by paired two-tailed *t*-test.

Acknowledgements
We dedicate this work to Elisa Izaurralde (1959–2018). We thank Catia Igreja and Dipankar Bhandari from Elisa Izaurralde's laboratory for generous advice on tethering and pull-down assays. We deeply thank Anabella Srebrow (IFIBYNE-UBA-CONICET, Argentina) for her generous support. We thank Dr Daniel Francés (IFISE-CONICET, Rosario, Argentina) for kindly helping with AMPK phosphorylation assays and Marina Fuertes Agudo (IBV-CSIC) for advice on blue-native gels. We are grateful to Andrés Rossi (Instituto Leloir) for assistance in confocal imaging, to Marcelo Perez-Pepe for advice in puromycilation assays and David A. Mancilla for help with *in silico* analysis.

Competing interests
The authors declare no competing or financial interests.

Author contributions
Conceptualization: A.J.F.-A., M.G.T., M.L.P., J.P., H.E.G., G.L.B., A.P.; Methodology: A.J.F.-A., M.G.T., M.L.P., M.H., J.P., A.A.C., P.E.L.S., L.B., M. Carmo-Fonseca, H.E.G., M. Casado, G.L.B.; Software: M.H., A.A.C., H.E.G.; Validation: A.J.F.-A., M.G.T., M.L.P., L.B., G.L.B.; Formal analysis: A.J.F.-A., M.G.T., M.L.P., M.H., J.P., A.A.C., J.P.P., P.E.L.S., L.B., M. Carmo-Fonseca, H.E.G., M. Casado, G.L.B.; Investigation: A.J.F.-A., M.G.T., M.L.P., M.H., J.P., A.A.C., J.P.P., P.E.L.S., L.B., M. Casado; Resources: H.E.G., M. Carmo-Fonseca, A.P., M. Casado, G.L.B.; Data curation: A.J.F.-A., M.G.T., A.A.C., H.E.G., M. Casado, G.L.B.; Writing - original draft: A.J.F.-A., M.G.T., M. Casado, G.L.B.; Writing - review & editing: A.J.F.-A., M.G.T., A.P., M. Carmo-Fonseca, H.E.G., G.L.B.; Visualization: G.L.B.; Supervision: A.J.F.-A., M.G.T., J.P.P., M. Carmo-Fonseca, H.E.G., G.L.B.; Project administration: G.L.B.; Funding acquisition: A.J.F.-A., M.G.T., A.P., M. Carmo-Fonseca, H.E.G., M. Casado, G.L.B.

Funding
This work was supported by the following grants: PICT 2013-3280 to G.L.B.; PICT 2014-3658 to G.L.B. and H.E.G.; PICT 2013-1301 to H.E.G.; PICT 2015-1302 to A.J.F.-A.; PICT 2012-2493 to M.G.T., PICT 2018-01790 to M.G.T. and A.J.F.-A., all from Agencia Nacional de Promoción Científica y Tecnológica (ANPCyT; Argentina); PIP2011-205 (Consejo Nacional de Investigaciones Científicas y Técnicas, CONICET, Argentina) to M.G.T.; an Alicia Moreau Chair from Paris Diderot University (France) to G.L.B. and A14S03 to G.L.B. and A.P. (MINCYT-ECOS SUD, Ministerio de Ciencia, Tecnología e Innovación Productiva); grant 1112 from the Fondation ARC pour la Recherche sur le Cancer to A.P., and SAF2016-75004-R (Ministerio de Economía, Industria y Competitividad, Gobierno de España; MINECO, Spain) and PROMETEO/2018/055 (Generalitat Valenciana, Spain) to M.C. M.C. participates in COST Action CA15203 MITOEAGLE. A.J.F.-A., M.G.T., H.G. and G.L.B. are investigators from CONICET, G.L.B. and H.E.G. are professors at the University of Buenos Aires, Argentina; M.L.P., M.H., P.E.L.S., J.P. and A.A.C. received fellowships from CONICET, J.P. visited Carmo Fonseca's Lab supported by H2020-Marie Sklodowska-Curie Research and Innovation Staff Exchanges [734825-LysoMod], A.P. is a professor at the University Paris Diderot.

Peer review history
The peer review history is available online at https://journals.biologists.com/jcs/article-lookup/doi/10.1242/jcs.253591.

References

Amadei, G., Vessey, J. P., Lipshitz, H. D., Smibert, C. A., Kaplan, D. R. and Miller, F. D. (2015a). The translational repressor Smaug2 regulates maintenance of mammalian neural stem cells. *Int. J. Dev. Neurosci.* **47**, 15. doi:10.1016/j.ijdevneu.2015.04.051

Amadei, G., Zander, M. A., Yang, G., Dumelie, J. G., Vessey, J. P., Lipshitz, H. D., Smibert, C. A., Kaplan, D. R. and Miller, F. D. (2015b). A Smaug2-based translational repression complex determines the balance between precursor maintenance versus differentiation during mammalian neurogenesis. *J. Neurosci.* **35**, 15666-15681. doi:10.1523/JNEUROSCI.2172-15.2015

Aviv, T., Lin, Z., Lau, S., Rendl, L. M., Sicheri, F. and Smibert, C. A. (2003). The RNA-binding SAM domain of Smaug defines a new family of post-transcriptional regulators. *Nat. Struct. Biol.* **10**, 614-621. doi:10.1038/nsb956

Aviv, T., Lin, Z., Ben-Ari, G., Smibert, C. A. and Sicheri, F. (2006). Sequence-specific recognition of RNA hairpins by the SAM domain of Vts1p. *Nat. Struct. Mol. Biol.* **13**, 168-176. doi:10.1038/nsmb1053

Baez, M. V. and Boccaccio, G. L. (2005). Mammalian Smaug is a translational repressor that forms cytoplasmic foci similar to stress granules. *J. Biol. Chem.* **280**, 43131-43140. doi:10.1074/jbc.M508374200

Baez, M. V., Luchelli, L., Maschi, D., Habif, M., Pascual, M., Thomas, M. G. and Boccaccio, G. L. (2011). Smaug1 mRNA-silencing foci respond to NMDA and modulate synapse formation. *J. Cell Biol.* **195**, 1141-1157. doi:10.1083/jcb.201108159

Béthune, J., Jansen, R.-P., Feldbrügge, M. and Zarnack, K. (2019). Membrane-associated RNA-binding proteins orchestrate organelle-coupled translation. *Trends Cell Biol.* **29**, 178-188. doi:10.1016/j.tcb.2018.10.005

Bhandari, D., Raisch, T., Weichenrieder, O., Jonas, S. and Izaurralde, E. (2014). Structural basis for the Nanos-mediated recruitment of the CCR4-NOT complex and translational repression. *Genes Dev.* **28**, 888-901. doi:10.1101/gad.237289.113

Bieman, M. A. (2014). Mechanism of Repression by the Sequence-Specific mRNA-Binding Protein Vts1p. PhD *Thesis*, Department of Biochemistry. University of Toronto. https://tspace.library.utoronto.ca/bitstream/1807/72599/1/Bieman_Melissa_201406_PhD_thesis.pdf

Bruzzone, L., Argüelles, C., Sanial, M., Miled, S., Alvisi, G., Gonçalves-Antunes, M., Qasrawi, F., Holmgren, R. A., Smibert, C. A., Lipshitz, H. D. et al. (2020). Regulation of the RNA-binding protein Smaug by the GPCR Smoothened via the kinase Fused. *EMBO Rep.* **21**, e48425. doi:10.15252/embr.201948425

Buchan, J. R. and Parker, R. (2009). Eukaryotic stress granules: the ins and outs of translation. *Mol. Cell* **36**, 932-941. doi:10.1016/j.molcel.2009.11.020

Cao, W. X., Kabelitz, S., Gupta, M., Yeung, E., Lin, S., Rammelt, C., Ihling, C., Pekovic, F., Low, T. C. H., Siddiqui, N. U. et al. (2020). Precise temporal regulation of post-transcriptional repressors is required for an orderly *Drosophila* maternal-to-Zygotic transition. *Cell Rep.* **31**, 107783. doi:10.1016/j.celrep.2020.107783

Chakravarty, A. K., Smejkal, T., Itakura, A. K., Garcia, D. M. and Jarosz, D. F. (2020). A non-amyloid prion particle that activates a heritable gene expression program. *Mol. Cell* **77**, 251-265.e9. doi:10.1016/j.molcel.2019.10.028

Chartier, A., Klein, P., Pierson, S., Barbezier, N., Gidaro, T., Casas, F., Carberry, S., Dowling, P., Maynadier, L., Bellec, M. et al. (2015). Mitochondrial dysfunction reveals the role of mRNA poly(A) tail regulation in oculopharyngeal muscular dystrophy pathogenesis. *PLoS Genet.* **11**, e1005092. doi:10.1371/journal.pgen.1005092

Chen, L., Dumelie, J. G., Li, X., Cheng, M. H., Yang, Z., Laver, J. D., Siddiqui, N. U., Westwood, J. T., Morris, Q., Lipshitz, H. D. et al. (2014a). Global regulation of mRNA translation and stability in the early *Drosophila* embryo by the Smaug RNA-binding protein. *Genome Biol.* **15**, R4. doi:10.1186/gb-2014-15-1-r4

Chen, Z., Holland, W., Shelton, J. M., Ali, A., Zhan, X., Won, S., Tomisato, W., Liu, C., Li, X., Moresco, E. M. Y. et al. (2014b). Mutation of mouse Samd4 causes leanness, myopathy, uncoupled mitochondrial respiration, and dysregulated mTORC1 signaling. *Proc. Natl. Acad. Sci. USA* **111**, 7367-7372. doi:10.1073/pnas.1406511111

Courchaine, E. M., Lu, A. and Neugebauer, K. M. (2016). Droplet organelles? *EMBO J.* **35**, 1603-1612. doi:10.15252/embj.201593517

D'Amico, D., Mottis, A., Potenza, F., Sorrentino, V., Li, H., Romani, M., Lemos, V., Schoonjans, K., Zamboni, N., Knott, G. et al. (2019). The RNA-binding protein PUM2 impairs mitochondrial dynamics and mitophagy during aging. *Mol. Cell* **73**, 775-787.e10. doi:10.1016/j.molcel.2018.11.034

de Haro, M., Al-Ramahi, I., Jones, K. R., Holth, J. K., Timchenko, L. T. and Botas, J. (2013). Smaug/SAMD4A restores translational activity of CUGBP1 and suppresses CUG-induced myopathy. *PLoS Genet.* **9**, e1003445. doi:10.1371/journal.pgen.1003445

Denes, L. T., Kelley, C. P. and Wang, E. T. (2021). Microtubule-based transport is essential to distribute RNA and nascent protein in skeletal muscle. *Nat. Commun.* **12**, 6079. doi:10.1038/s41467-021-26383-9.

Deng, L., Yang, S.-B., Xu, F.-F. and Zhang, J.-H. (2015). Long noncoding RNA CCAT1 promotes hepatocellular carcinoma progression by functioning as let-7 sponge. *J. Exp. Clin. Cancer Res.* **34**, 18. doi:10.1186/s13046-015-0136-7

Doerrier, C., Garcia-Souza, L. F., Krumschnabel, G., Wohlfarter, Y., Mészáros, A. T. and Gnaiger, E. (2018). High-resolution FluoRespirometry and OXPHOS protocols for human cells, permeabilized fibers from small biopsies of muscle, and isolated mitochondria. *Methods Mol. Biol.* **1782**, 31-70. doi:10.1007/978-1-4939-7831-1_3

Ehses, S., Raschke, I., Mancuso, G., Bernacchia, A., Geimer, S., Tondera, D., Martinou, J.-C., Westermann, B., Rugarli, E. I. and Langer, T. (2009). Regulation of OPA1 processing and mitochondrial fusion by m-AAA protease isoenzymes and OMA1. *J. Cell Biol.* **187**, 1023-1036. doi:10.1083/jcb.200906084

Eichhorn, S. W., Subtelny, A. O., Kronja, I., Kwasnieski, J. C., Orr-Weaver, T. L. and Bartel, D. P. (2016). mRNA poly(A)-tail changes specified by deadenylation broadly reshape translation in Drosophila oocytes and early embryos. *eLife* **5**, e16955. doi:10.7554/eLife.16955

Enam, S. U., Zinshteyn, B., Goldman, D. H., Cassani, M., Livingston, N. M., Seydoux, G. and Green, R. (2020). Puromycin reactivity does not accurately localize translation at the subcellular level. *eLife* **9**, e60303. doi:10.7554/eLife.60303

Fernández-Alvarez, A. J., Pascual, M. L., Boccaccio, G. L. and Thomas, M. G. (2016). Smaug variants in neural and non-neuronal cells. *Commun. Integr. Biol.* **9**, e1139252. doi:10.1080/19420889.2016.1139252

Fessler, E., Eckl, E.-M., Schmitt, S., Mancilla, I. A., Meyer-Bender, M. F., Hanf, M., Philippou-Massier, J., Krebs, S., Zischka, H. and Jae, L. T. (2020). A pathway coordinated by DELE1 relays mitochondrial stress to the cytosol. *Nature* **579**, 433-437. doi:10.1038/s41586-020-2076-4

French, J. B., Jones, S. A., Deng, H., Pedley, A. M., Kim, D., Chan, C. Y., Hu, H., Pugh, R. J., Zhao, H., Zhang, Y. et al. (2016). Spatial colocalization and functional link of purinosomes with mitochondria. *Science* **351**, 733-737. doi:10.1126/science.aac6054

Friedman, J. R. and Nunnari, J. (2014). Mitochondrial form and function. *Nature* **505**, 335-343. doi:10.1038/nature12985

Gan, Z., Fu, T., Kelly, D. P. and Vega, R. B. (2018). Skeletal muscle mitochondrial remodeling in exercise and diseases. *Cell Res.* **28**, 969-980. doi:10.1038/s41422-018-0078-7

Gao, J., Schatton, D., Martinelli, P., Hansen, H., Pla-Martin, D., Barth, E., Becker, C., Altmueller, J., Frommolt, P., Sardiello, M. et al. (2014). CLUH regulates mitochondrial biogenesis by binding mRNAs of nuclear-encoded mitochondrial proteins. *J. Cell Biol.* **207**, 213-223. doi:10.1083/jcb.201403129

Gehrke, S., Wu, Z., Klinkenberg, M., Sun, Y., Auburger, G., Guo, S. and Lu, B. (2015). PINK1 and Parkin control localized translation of respiratory chain component mRNAs on mitochondria outer membrane. *Cell Metab.* **21**, 95-108. doi:10.1016/j.cmet.2014.12.007

Gnaiger, E. (2020). Mitochondrial pathways and respiratory control. In *An introduction to OXPHOS analysis* (5th ed. Bioenerg Commun 2: 122 pp). doi:10.26124/bec:2020-0002

Green, J. B., Gardner, C. D., Wharton, R. P. and Aggarwal, A. K. (2003). RNA recognition via the SAM domain of Smaug. *Mol. Cell* **11**, 1537-1548. doi:10.1016/S1097-2765(03)00178-3

Guo, L. and Shorter, J. (2015). It's raining liquids: rna tunes viscoelasticity and dynamics of membraneless organelles. *Mol. Cell* **60**, 189-192. doi:10.1016/j.molcel.2015.10.006

Hawley, S. A., Gadalla, A. E., Olsen, G. S. and Hardie, D. G. (2002). The antidiabetic drug metformin activates the AMP-activated protein kinase cascade via an adenine nucleotide-independent mechanism. *Diabetes* **51**, 2420-2425. doi:10.2337/diabetes.51.8.2420

Hoppins, S., Lackner, L. and Nunnari, J. (2007). The machines that divide and fuse mitochondria. *Annu. Rev. Biochem.* **76**, 751-780. doi:10.1146/annurev.biochem.76.071905.090048

Howell, J. J., Hellberg, K., Turner, M., Talbott, G., Kolar, M. J., Ross, D. S., Ross, D. S., Hoxhaj, G., Saghatelian, A., Shaw, R. J. et al. (2017). Metformin inhibits hepatic mTORC1 signaling via dose-dependent mechanisms involving AMPK and the TSC complex. *Cell Metab.* **25**, 463-471. doi:10.1016/j.cmet.2016.12.009

Hubstenberger, A., Courel, M., Bénard, M., Souquere, S., Ernoult-Lange, M., Chouaib, R., Yi, Z., Morlot, J.-B., Munier, A., Fradet, M. et al. (2017). P-body purification reveals the condensation of repressed mRNA regulons. *Mol. Cell* **68**, 144-157.e5. doi:10.1016/j.molcel.2017.09.003

Izzo, A., Nitti, M., Mollo, N., Paladino, S., Procaccini, C., Faicchia, D., Calì, G., Genesio, R., Bonfiglio, F., Cicatiello, R. et al. (2017). Metformin restores the mitochondrial network and reverses mitochondrial dysfunction in Down syndrome cells. *Hum. Mol. Genet.* **26**, 1056-1069. doi:10.1093/hmg/ddx016

Johnson, P. E. and Donaldson, L. W. (2006). RNA recognition by the Vts1p SAM domain. *Nat. Struct. Mol. Biol.* **13**, 177-178. doi:10.1038/nsmb1039

Kalender, A., Selvaraj, A., Kim, S. Y., Gulati, P., Brûlé, S., Viollet, B., Kemp, B. E., Bardeesy, N., Dennis, P., Schlager, J. J. et al. (2010). Metformin, independent of AMPK, inhibits mTORC1 in a rag GTPase-dependent manner. *Cell Metab.* **11**, 390-401. doi:10.1016/j.cmet.2010.03.014

Kedersha, N., Chen, S., Gilks, N., Li, W., Miller, I. J., Stahl, J. and Anderson, P. (2002). Evidence that ternary complex (eIF2-GTP-tRNA$_i^{Met}$)-deficient preinitiation complexes are core constituents of mammalian stress granules. *Mol. Biol. Cell* **13**, 1-391. doi:10.1091/mbc.01-05-0221

Khong, A. and Parker, R. (2018). mRNP architecture in translating and stress conditions reveals an ordered pathway of mRNP compaction. *J. Cell Biol.* **217**, 4124-4140. doi:10.1083/jcb.201806183

Kopp, F., Elguindy, M. M., Yalvac, M. E., Zhang, H., Chen, B., Gillett, F. A., Lee, S., Sivakumar, S., Yu, H., Xie, Y. et al. (2019). PUMILIO hyperactivity drives premature aging of Norad-deficient mice. *eLife* **8**, e42650. doi:10.7554/eLife.42650

Kriaucionis, S., Paterson, A., Curtis, J., Guy, J., Macleod, N. and Bird, A. (2006). Gene expression analysis exposes mitochondrial abnormalities in a mouse model of Rett syndrome. *Mol. Cell Biol.* **26**, 5033-5042. doi:10.1128/MCB.01665-05

Kuzniewska, B., Cysewski, D., Wasilewski, M., Sakowska, P., Milek, J., Kulinski, T. M., Winiarski, M., Kozielewicz, P., Knapska, E., Dadlez, M. et al. (2020). Mitochondrial protein biogenesis in the synapse is supported by local translation. *EMBO Rep.* **21**, e48882. doi:10.15252/embr.201948882

Larsson, O., Morita, M., Topisirovic, I., Alain, T., Blouin, M.-J., Pollak, M. and Sonenberg, N. (2012). Distinct perturbation of the translatome by the antidiabetic drug metformin. *Proc. Natl. Acad. Sci. USA* **109**, 8977-8982. doi:10.1073/pnas.1201689109

Laver, J. D., Ancevicius, K., Sollazzo, P., Westwood, J. T., Sidhu, S. S., Lipshitz, H. D. and Smibert, C. A. (2012). Synthetic antibodies as tools to probe RNA-binding protein function. *Mol. Biosyst.* **8**, 1650-1657. doi:10.1039/c2mb00007e

Lee, C.-D. and Tu, B. P. (2015). Glucose-regulated phosphorylation of the PUF protein Puf3 regulates the translational fate of its bound mRNAs and association with RNA granules. *Cell Rep.* **11**, 1638-1650. doi:10.1016/j.celrep.2015.05.014

Luchelli, L., Thomas, M. G. and Boccaccio, G. L. (2015). Synaptic control of mRNA translation by reversible assembly of XRN1 bodies. *J. Cell Sci.* **128**, 1542-1554. doi:10.1242/jcs.163295

Lykke-Andersen, J., Shu, M.-D. and Steitz, J. A. (2000). Human Upf proteins target an mRNA for nonsense-mediated decay when bound downstream of a termination codon. *Cell* **103**, 1121-1131. doi:10.1016/S0092-8674(00)00214-2

Ma, W. and Mayr, C. (2018). A membraneless organelle associated with the endoplasmic reticulum enables 3′UTR-mediated protein-protein interactions. *Cell* **175**, 1492-1506.e19. doi:10.1016/j.cell.2018.10.007

Malik-Sheriff, R. S., Imtiaz, S., Grecco, H. E. and Zamir, E. (2018). Diverse patterns of molecular changes in the mechano-responsiveness of focal adhesions. *Sci. Rep.* **8**, 2187. doi:10.1038/s41598-018-20252-0

Moon, S. L., Morisaki, T., Khong, A., Lyon, K., Parker, R. and Stasevich, T. J. (2019). Multicolour single-molecule tracking of mRNA interactions with RNP granules. *Nat. Cell Biol.* **21**, 162-168. doi:10.1038/s41556-018-0263-4

Moosavi, B., Berry, E. A., Zhu, X.-L., Yang, W.-C. and Yang, G.-F. (2019). The assembly of succinate dehydrogenase: a key enzyme in bioenergetics. *Cell Mol. Life Sci.* **76**, 4023-4042. doi:10.1007/s00018-019-03200-7

Morita, M., Gravel, S.-P., Chénard, V., Sikström, K., Zheng, L., Alain, T., Gandin, V., Avizonis, D., Arguello, M., Zakaria, C. et al. (2013). mTORC1 controls mitochondrial activity and biogenesis through 4E-BP-dependent translational regulation. *Cell Metab.* **18**, 698-711. doi:10.1016/j.cmet.2013.10.001

Nelson, M. R., Leidal, A. M. and Smibert, C. A. (2004). *Drosophila* Cup is an eIF4E-binding protein that functions in Smaug-mediated translational repression. *EMBO J.* **23**, 150-159. doi:10.1038/sj.emboj.7600026

Niu, N., Xiang, J.-F., Yang, Q., Wang, L., Wei, Z., Chen, L.-L., Yang, L. and Zou, W. (2017). RNA-binding protein SAMD4 regulates skeleton development through translational inhibition of Mig6 expression. *Cell Discov.* **3**, 16050. doi:10.1038/celldisc.2016.50

Oberstrass, F. C., Lee, A., Stefl, R., Janis, M., Chanfreau, G. and Allain, F. H.-T. (2006). Shape-specific recognition in the structure of the Vts1p SAM domain with RNA. *Nat. Struct. Mol. Biol.* **13**, 160-167. doi:10.1038/nsmb1038

Olivas, W. and Parker, R. (2000). The Puf3 protein is a transcript-specific regulator of mRNA degradation in yeast. *EMBO J.* **19**, 6602-6611. doi:10.1093/emboj/19.23.6602

Perez-Pepe, M., Fernández-Alvarez, A. J. and Boccaccio, G. L. (2018). Life and work of stress granules and processing bodies: new insights into their formation and function. *Biochemistry* **57**, 2488-2498. doi:10.1021/acs.biochem.8b00025

Pinder, B. D. and Smibert, C. A. (2013). microRNA-independent recruitment of Argonaute 1 to nanos mRNA through the Smaug RNA-binding protein. *EMBO Rep.* **14**, 80-86. doi:10.1038/embor.2012.192

Pitts, K. R., Yoon, Y., Krueger, E. W. and McNiven, M. A. (1999). The dynamin-like protein DLP1 is essential for normal distribution and morphology of the endoplasmic reticulum and mitochondria in mammalian cells. *Mol. Biol. Cell* **10**, 4403-4417. doi:10.1091/mbc.10.12.4403

Pla-Martín, D., Schatton, D., Wiederstein, J. L., Marx, M.-C., Khiati, S., Krüger, M. and Rugarli, E. I. (2020). CLUH granules coordinate translation of mitochondrial proteins with mTORC1 signaling and mitophagy. *EMBO J.* **39**, e102731. doi:10.15252/embj.2019102731

Rangaraju, V., Lauterbach, M. and Schuman, E. M. (2019). Spatially stable mitochondrial compartments fuel local translation during plasticity. *Cell* **176**, 73-84.e15. doi:10.1016/j.cell.2018.12.013

Rouget, C., Papin, C., Boureux, A., Meunier, A.-C., Franco, B., Robine, N., Lai, E. C., Pelisson, A. and Simonelig, M. (2010). Maternal mRNA deadenylation and decay by the piRNA pathway in the early *Drosophila* embryo. *Nature* **467**, 1128-1132. doi:10.1038/nature09465

Rugarli, E. I. and Langer, T. (2012). Mitochondrial quality control: a matter of life and death for neurons. *EMBO J.* **31**, 1336-1349. doi:10.1038/emboj.2012.38

Sachdev, R., Hondele, M., Linsenmeier, M., Vallotton, P., Mugler, C. F., Arosio, P. and Weis, K. (2019). Pat1 promotes processing body assembly by enhancing the phase separation of the DEAD-box ATPase Dhh1 and RNA. *eLife* **8**, e41415. doi:10.7554/eLife.41415

Schatton, D. and Rugarli, E. I. (2018). A concert of RNA-binding proteins coordinates mitochondrial function. *Crit. Rev. Biochem. Mol. Biol.* **53**, 652-666. doi:10.1080/10409238.2018.1553927

Schatton, D., Pla-Martin, D., Marx, M.-C., Hansen, H., Mourier, A., Nemazanyy, I., Pessia, A., Zentis, P., Corona, T., Kondylis, V. et al. (2017). CLUH regulates mitochondrial metabolism by controlling translation and decay of target mRNAs. *J. Cell Biol.* **216**, 675-693. doi:10.1083/jcb.201607019

Semotok, J. L., Cooperstock, R. L., Pinder, B. D., Vari, H. K., Lipshitz, H. D. and Smibert, C. A. (2005). Smaug recruits the CCR4/POP2/NOT deadenylase

complex to trigger maternal transcript localization in the early *Drosophila* embryo. *Curr. Biol.* **15**, 284-294. doi:10.1016/j.cub.2005.01.048

Semotok, J. L., Luo, H., Cooperstock, R. L., Karaiskakis, A., Vari, H. K., Smibert, C. A. and Lipshitz, H. D. (2008). *Drosophila* maternal Hsp83 mRNA destabilization is directed by multiple SMAUG recognition elements in the open reading frame. *Mol. Cell Biol.* **28**, 6757-6772. doi:10.1128/MCB.00037-08

Sgromo, A., Raisch, T., Bawankar, P., Bhandari, D., Chen, Y., Kuzuoğlu-Öztürk, D., Weichenrieder, O. and Izaurralde, E. (2017). A CAF40-binding motif facilitates recruitment of the CCR4-NOT complex to mRNAs targeted by *Drosophila* Roquin. *Nat. Commun.* **8**, 14307. doi:10.1038/ncomms14307

Shan, W., Li, J., Xu, W., Li, H. and Zuo, Z. (2019). Critical role of UQCRC1 in embryo survival, brain ischemic tolerance and normal cognition in mice. *Cell Mol. Life Sci.* **76**, 1381-1396. doi:10.1007/s00018-019-03007-6

She, R., Chakravarty, A. K., Layton, C. J., Chircus, L. M., Andreasson, J. O. L., Damaraju, N., McMahon, P. L., Buenrostro, J. D., Jarosz, D. F. and Greenleaf, W. J. (2017). Comprehensive and quantitative mapping of RNA-protein interactions across a transcribed eukaryotic genome. *Proc. Natl. Acad. Sci. USA* **114**, 3619-3624. doi:10.1073/pnas.1618370114

St-Pierre, J. and Topisirovic, I. (2016). Nucleus to mitochondria: lost in transcription, found in translation. *Dev. Cell* **37**, 490-492. doi:10.1016/j.devcel.2016.06.003

Tadros, W., Goldman, A. L., Babak, T., Menzies, F., Vardy, L., Orr-Weaver, T., Hughes, T. R., Westwood, J. T., Smibert, C. A. and Lipshitz, H. D. (2007). SMAUG is a major regulator of maternal mRNA destabilization in *Drosophila* and its translation is activated by the PAN GU kinase. *Dev. Cell* **12**, 143-155. doi:10.1016/j.devcel.2006.10.005

Tang, X., Orlicky, S., Lin, Z., Willems, A., Neculai, D., Ceccarelli, D., Mercurio, F., Shilton, B. H., Sicheri, F. and Tyers, M. (2007). Suprafacial orientation of the SCFCdc4 dimer accommodates multiple geometries for substrate ubiquitination. *Cell* **129**, 1165-1176. doi:10.1016/j.cell.2007.04.042

Thomas, M. G., Martinez Tosar, L. J., Loschi, M., Pasquini, J. M., Correale, J., Kindler, S. and Boccaccio, G. L. (2005). Staufen recruitment into stress granules does not affect early mRNA transport in oligodendrocytes. *Mol. Biol. Cell* **16**, 405-420. doi:10.1091/mbc.E04-06-0516

Thomas, M. G., Pascual, M. L., Maschi, D., Luchelli, L. and Boccaccio, G. L. (2014). Synaptic control of local translation: the plot thickens with new characters. *Cell Mol. Life Sci.* **71**, 2219-2239. doi:10.1007/s00018-013-1506-y

Tondera, D., Grandemange, S., Jourdain, A., Karbowski, M., Mattenberger, Y., Herzig, S., Da Cruz, S., Clerc, P., Raschke, I., Merkwirth, C. et al. (2009). SLP-2 is required for stress-induced mitochondrial hyperfusion. *EMBO J.* **28**, 1589-1600. doi:10.1038/emboj.2009.89

Toyama, E. Q., Herzig, S., Courchet, J., Lewis, T. L., Jr., Loson, O. C., Hellberg, K., Young, N. P., Chen, H., Polleux, F., Chan, D. C. et al. (2016). AMP-activated protein kinase mediates mitochondrial fission in response to energy stress. *Science* **351**, 275-281. doi:10.1126/science.aab4138

Unterholzner, L. and Izaurralde, E. (2004). SMG7 acts as a molecular link between mRNA surveillance and mRNA decay. *Mol. Cell* **16**, 587-596. doi:10.1016/j.molcel.2004.10.013

Van Treeck, B., Protter, D. S. W., Matheny, T., Khong, A., Link, C. D. and Parker, R. (2018). RNA self-assembly contributes to stress granule formation and defining the stress granule transcriptome. *Proc. Natl. Acad. Sci. USA* **115**, 2734-2739. doi:10.1073/pnas.1800038115

Vardi-Oknin, D. and Arava, Y. (2019). Characterization of factors involved in localized translation near mitochondria by ribosome-proximity labeling. *Front. Cell Dev. Biol.* **7**, 305. doi:10.3389/fcell.2019.00305

Vincent, T., Vingadassalon, A., Ubrig, E., Azeredo, K., Srour, O., Cognat, V., Graindorge, S., Salinas, T., Maréchal-Drouard, L. and Duchene, A.-M. (2017). A genome-scale analysis of mRNAs targeting to plant mitochondria: upstream AUGs in 5′ untranslated regions reduce mitochondrial association. *Plant J.* **92**, 1132-1142. doi:10.1111/tpj.13749

Wakim, J., Goudenege, D., Perrot, R., Gueguen, N., Desquiret-Dumas, V., Chao de la Barca, J. M., Dalla Rosa, I., Manero, F., Le Mao, M., Chupin, S. et al. (2017). CLUH couples mitochondrial distribution to the energetic and metabolic status. *J. Cell Sci.* **130**, 1940-1951. doi:10.1242/jcs.201616

Wang, Q., Zhang, M., Torres, G., Wu, S., Ouyang, C., Xie, Z. and Zou, M.-H. (2017). Metformin suppresses diabetes-accelerated atherosclerosis via the inhibition of Drp1-mediated mitochondrial fission. *Diabetes* **66**, 193-205. doi:10.2337/db16-0915

Wheaton, W. W., Weinberg, S. E., Hamanaka, R. B., Soberanes, S., Sullivan, L. B., Anso, E., Glasauer, A., Dufour, E., Mutlu, G. M., Budigner, G. R. S. et al. (2014). Metformin inhibits mitochondrial complex I of cancer cells to reduce tumorigenesis. *eLife* **3**, e02242. doi:10.7554/eLife.02242

Wilk, R., Hu, J., Blotsky, D. and Krause, H. M. (2016). Diverse and pervasive subcellular distributions for both coding and long noncoding RNAs. *Genes Dev.* **30**, 594-609. doi:10.1101/gad.276931.115

Williams, C. C., Jan, C. H. and Weissman, J. S. (2014). Targeting and plasticity of mitochondrial proteins revealed by proximity-specific ribosome profiling. *Science* **346**, 748-751. doi:10.1126/science.1257522

Wu, Z., Wang, Y., Lim, J., Liu, B., Li, Y., Vartak, R., Stankiewicz, T., Montgomery, S. and Lu, B. (2018). Ubiquitination of ABCE1 by NOT4 in response to mitochondrial damage links co-translational quality control to PINK1-directed mitophagy. *Cell Metab.* **28**, 130-144.e7. doi:10.1016/j.cmet.2018.05.007

Zhou, G., Myers, R., Li, Y., Chen, Y., Shen, X., Fenyk-Melody, J., Wu, M., Ventre, J., Doebber, T., Fujii, N. et al. (2001). Role of AMP-activated protein kinase in mechanism of metformin action. *J. Clin. Invest.* **108**, 1167-1174. doi:10.1172/JCI13505

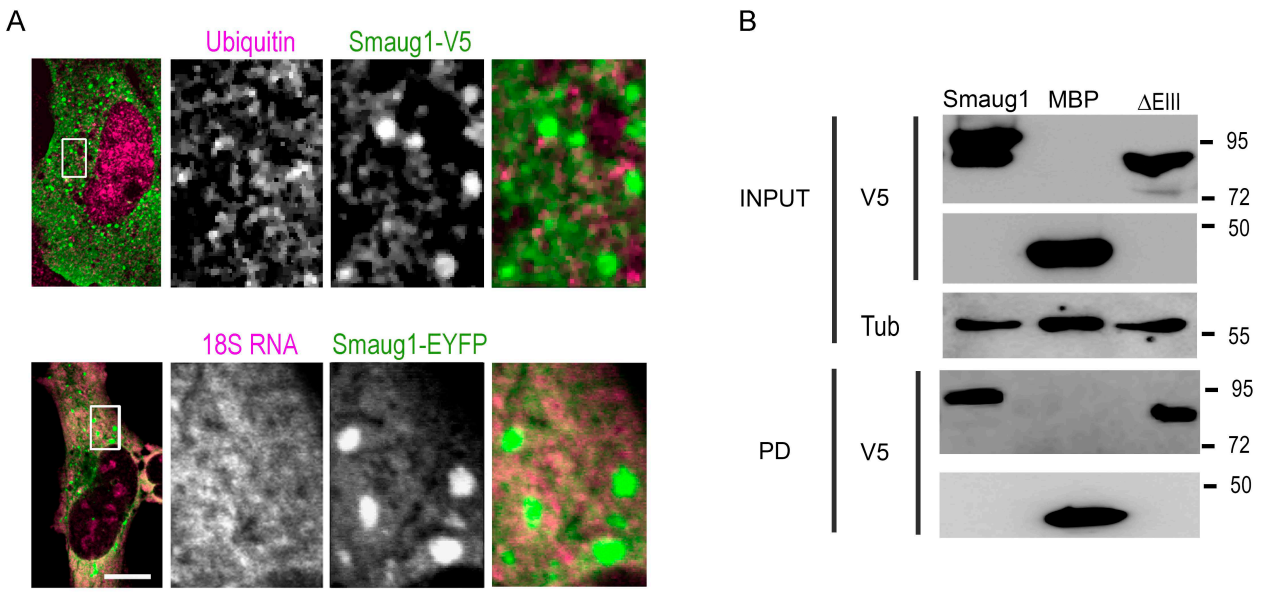

Fig. S1. A. Smaug1-EYFP bodies exclude ubiquitin and small ribosomal subunits (linked to Figure 1C). Top, Smaug1-V5-transfected U2OS cells were immunostained for V5 and ubiquitin. Bottom, FISH with a ribosomal 18S riboprobe was performed in Smaug1-EYFP-transfected cells as described in Materials and Methods**.** Representative images from two independent stainings are shown in each case. Both ubiquitin and 18S rRNA are excluded from Smaug1-EYFP bodies.

B. Expression levels and recovery of Smaug1 constructs (linked to Figure 1D). Expression levels of the indicated constructs tagged with MBP-V5 and their recovery after pull-down were analyzed by western blot using an anti-V5 antibody. Tubulin was used as loading control for the input samples.

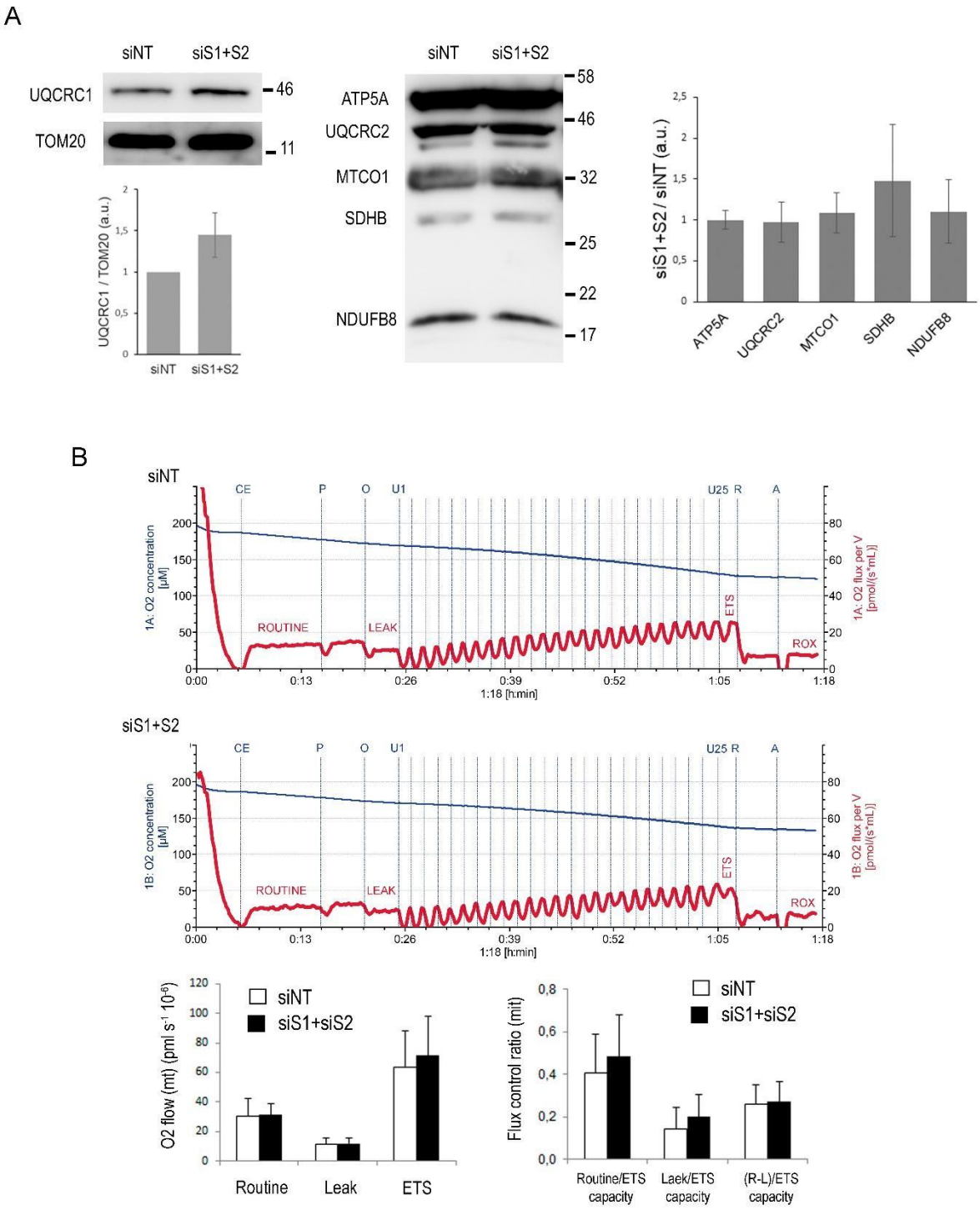

Fig. S2. A Expression levels of mitochondrial enzymes upon Smaug1+2 knockdown. The indicated proteins were analyzed by western blot of mitochondrial protein extracts obtained as described in Materials and Methods. Three independent experiments were performed and the media value is plotted. A representative image is shown. Error bars, standard deviation.

B. Respiratory capacity of Smaug1+2 knockdown U2O2 cells (linked to Figure 2C) U2OS were treated with non-targeting (NT) siRNA or with siRNAs against both Smaug1 and Smaug2 (siS1+S2) and respiration in intact cells (1×10^6 cells/mL) was examined in growth medium at 37 °C as described in Materials and Methods. Oxygen flow (pmol $O_2 \times s^{-1} \times 10^{-6}$ cells) and total oxygen concentration (nmol/mL) in the Oxygraph chamber are indicated as red and blue traces, respectively. CE: cellular substrate, P: Pyruvate, O: Oligomycin, U: Uncoupler (CCCP) R: Rotenone, A: Antimycin A. After measuring routine oxygen consumption, the adenosine triphosphate (ATP)-synthase inhibitor oligomycin was added to evaluate proton LEAK. The uncoupler carbonyl cyanide m-chlorophenylhydrazone (CCCP) allowed the measurement of maximal oxygen consumption (Max) stimulating maximal respiration assuming all required substrates are present. Finally, rotenone (complex I inhibitor) and antimycin A (complex III inhibitor), which completely prevent oxygen consumption through the ETC were added. Oxygen flow per cell was corrected for ROX at the indicated mitochondrial respiration state. Calculated mitochondrial (mt) flux control ratios show basal cellular routine respiration (R), leak respiration (L) and fraction of respiration (netR = R-L) used for ATP production normalized to ETS capacity.

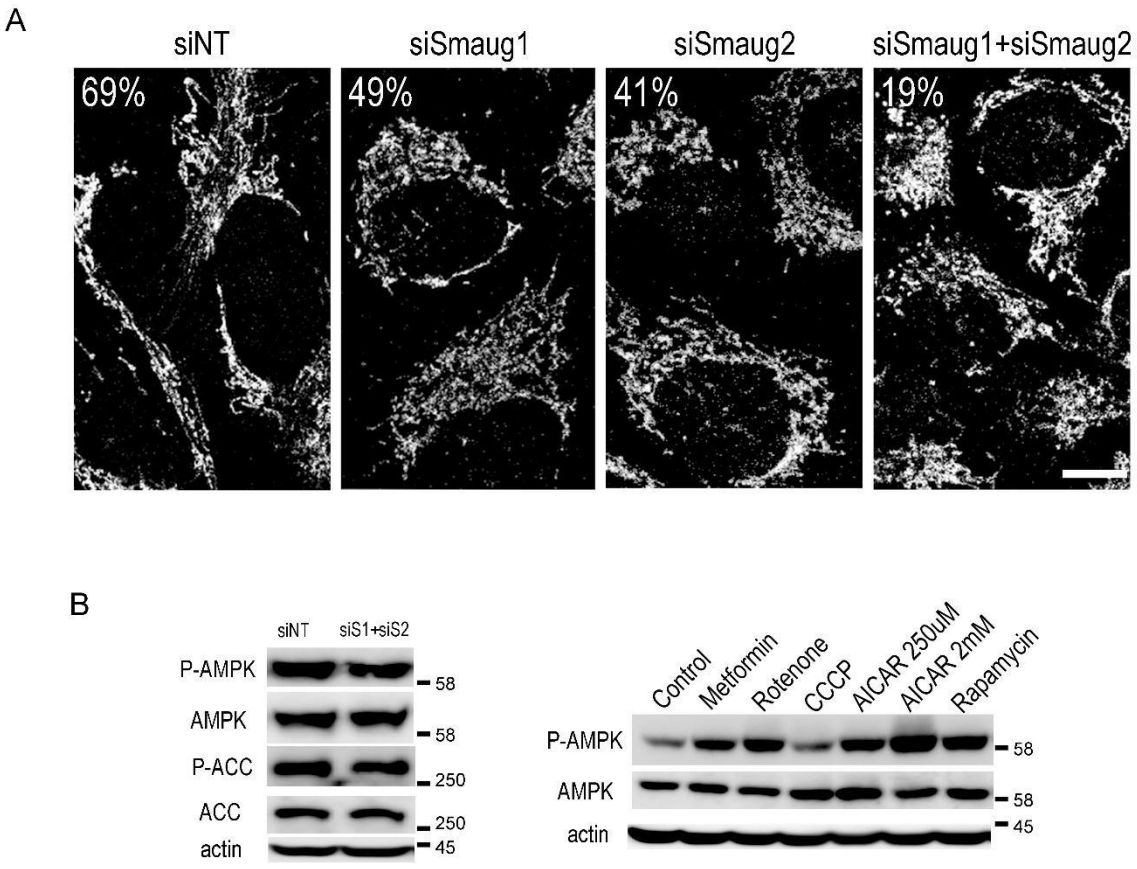

Fig. S3. A Mitochondrial network disruption upon Smaug1 and Smaug2 knockdown (linked to Figure 3A). U2OS cells were treated with the indicated siRNAs and live-stained with MitoTracker™ Red CMXRos. At least 200 cells per treatment were analyzed and the percentage of cells with elongated mitochondria is indicated. A representative experiment out of three is shown. Scale bars, 10 μm.

B. Phosphorylation levels of AMPK and ACC remained unchanged upon Smaug1+2 knockdown. U2OS cells were treated with the indicated siRNAs or exposed to metformin, AICAR or rapamycin. Whole cell protein extracts were obtained by lysis with 1XSDS loading buffer as described in Materials and Methods. Phosphorylation of AMPKα and of its target ACC, and their total protein levels were analyzed by western blot. Three independent experiments were performed and a representative western blot is shown.

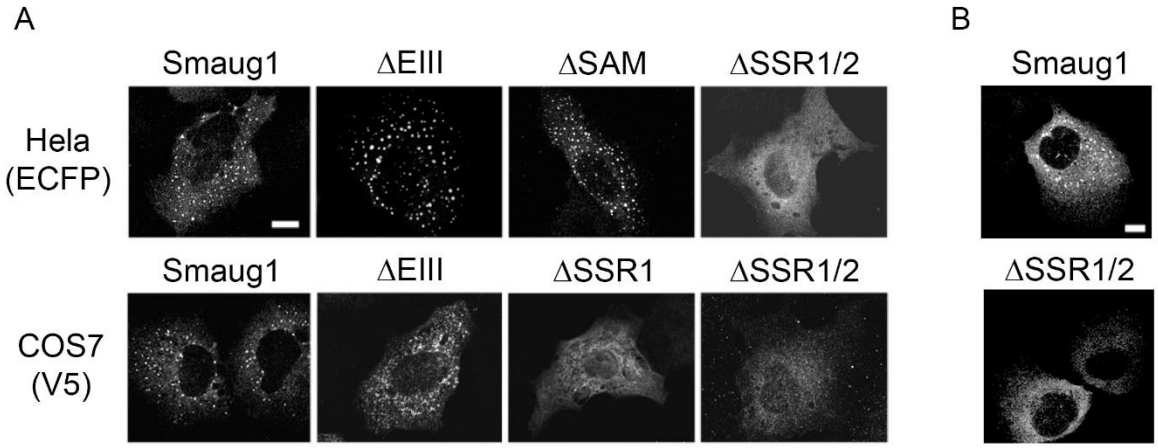

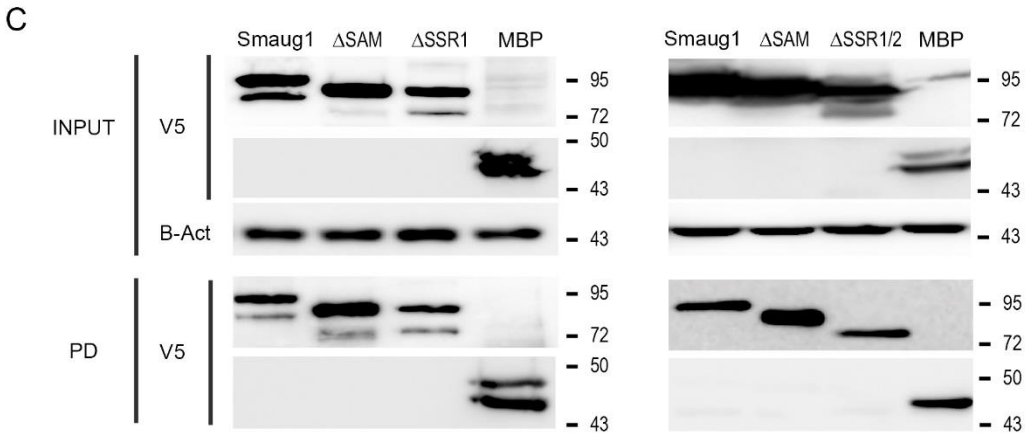

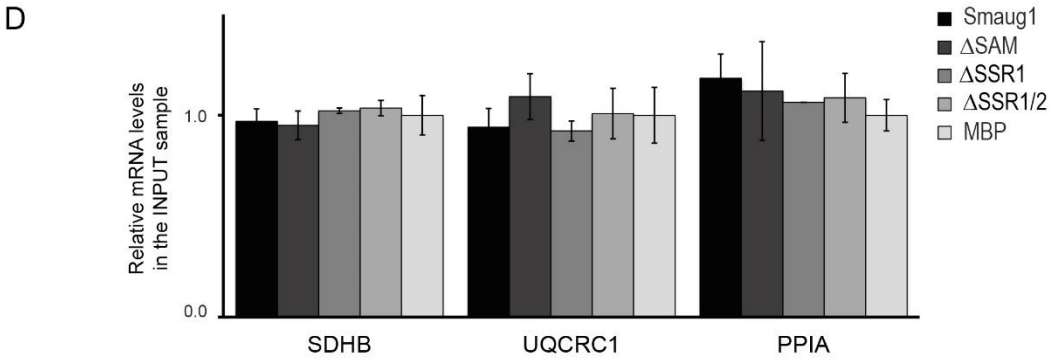

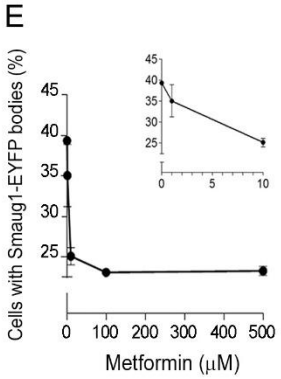

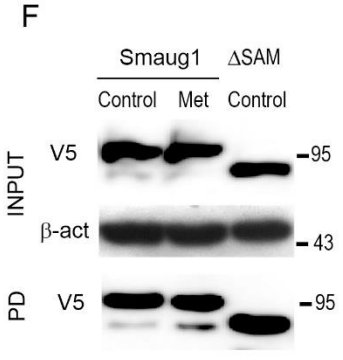

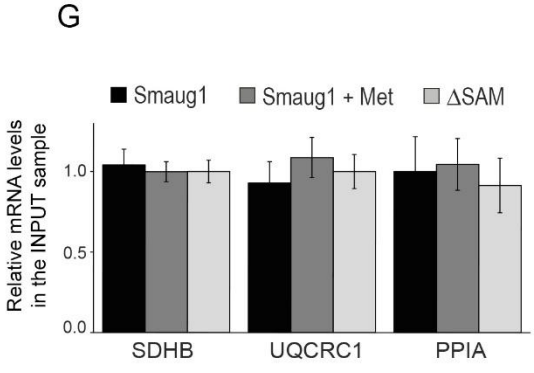

Fig. S4. A Smaug-MLO formation in COS7 and HeLa cells (linked to Figure 5D). Representative images of cells transfected with the indicated constructs tagged with V5-SBP or ECFP are shown. At least two independent transfection experiments were performed in each case.

B Smaug MLO formation in tethering assay (linked to Figure 6B). U2Os cells were co-transfected with the firefly reporter carrying a tandem array of 6 MS2 binding sites and the indicated constructs tagged with MS2-HA. Three independent experiments were performed and representative cells are depicted .

C,D Expression levels of Smaug1 constructs and target mRNAs (linked to Figure 6C). (C) Expression levels of the indicated constructs tagged with MBP-V5 and their recovery after pull-down were analyzed by western blot using anti-V5 antibody. β-actin was used as loading control for the input samples. **(D)** Levels of the indicated transcripts in the input samples depicted in Figure 6C were determined by RT-qPCR and normalized to RpLp0 mRNA values.

E Response to metformin in U2OS cells. Cells transfected with Smaug1-EYFP were exposed during 1 h at the indicated metformin concentrations. More than 100 cells from duplicate coverslips were analyzed for each experimental point. Error bars, standard deviation.

F,G Expression levels of Smaug1 constructs and of target mRNAs upon metformin treatment (linked to Figure 8C). (F) Western blot of input and pull-down (PD) samples depicted in Figure 8C. **(G)** Levels of the indicated transcripts in the input samples depicted in Figure 8C were determined by RT-qPCR and normalized to RpLp0 mRNA values.

Table S1. A putative mitochondrial regulon linked to Smaug

Chen et al. (2014) reported 340 transcripts bound to Smaug and 1918 mRNAs translationally repressed by Smaug in Drosophila embryos (additional data files 2 and 7 in (Chen et al., 2014)). Among these Smaug targets, several mRNAs are linked to mitochondrial function. In addition, Chartier et al. (2015) reported that mRNAs of TCE components are bound to Drosophila Smaug in adult thorax (Chartier et al., 2015).

Fucntion	Name		REF
ETC	SDHB	bound	mammalian U2OS cells (this work)
ETC	UQCRC1	bound, repressed?	mammalian U2OS cells (this work)
ACYL-COA DEHYDROGENASES	Butyryl-CoA dehydrogenase;DmelCG6638;ortholog	bound, repressed	Drosphila embryo (Chen et al., 2014)
alpha-amino acid metabolicprocess	Probable methylmalonate-semialdehyde dehydrogenase [acylating], mitochondrial;FlyBase:FBgn0023537;ortholog	bound, repressed	Drosphila embryo (Chen et al., 2014)
ETC	Succinate dehydrogenase [ubiquinone] flavoprotein subunit, mitochondrial;SdhA;ortholog	bound, repressed	Drosphila embryo (Chen et al., 2014)
ETC	Ferrochelatase, mitochondrial;FeCh;ortholog	bound, repressed	Drosphila embryo (Chen et al., 2014)
ETC and OXPHOS	BcDNA. GH02220;OXA1L;ortholog	bound, repressed	Drosphila embryo (Chen et al., 2014)
fatty acid beta-oxidation	GH06693p;152078_at;ortholog	bound, repressed	Drosphila embryo (Chen et al., 2014)
fatty acid catabolic process	Arc42;Arc42;ortholog	bound, repressed	Drosphila embryo (Chen et al., 2014)
iron-sulfur cluster assembly-ETC related process	Cysteine desulfurase, mitochondrial;Nfs1;ortholog	bound, repressed	Drosphila embryo (Chen et al., 2014)
mis c	RE48077p;BNIP3;ortholog	bound, repressed	Drosphila embryo (Chen et al., 2014)
mis c	ATG11 domain-containing protein;Atg17;ortholog	bound, repressed	Drosphila embryo (Chen et al., 2014)
mitochondrial translation	Mitochondrial ribosomal protein L38;mRpL38;ortholog	bound, repressed	Drosphila embryo (Chen et al., 2014)
mitochondrial translation	Probable 28S ribosomal protein S25, mitochondrial;mRpS25;ortholog	bound, repressed	Drosphila embryo (Chen et al., 2014)
mitochondrial translation	CG6459 protein;P32;ortholog	bound, repressed	Drosphila embryo (Chen et al., 2014)
mitochondrial translation	Mitochondrial ribosomal protein L53;mRpL53;ortholog	bound, repressed	Drosphila embryo (Chen et al., 2014)
OxPhos	ATP synthase subunit beta, mitochondrial;ATPsynbeta;ortholog	bound, repressed	Drosphila embryo (Chen et al., 2014)
OxPhos	ATP synthase subunit alpha, mitochondrial;blw;ortholog	bound, repressed	Drosphila embryo (Chen et al., 2014)
protein import	Mitochondrial import inner membrane translocase subunit TIM44;CG11799;ortholog	bound, repressed	Drosphila embryo (Chen et al., 2014)
protein import	CHCH domain-containing protein;DmelCG7950;ortholog	bound, repressed	Drosphila embryo (Chen et al., 2014)
pyruvate metabolic process	Pyruvate dehydrogenase E1 component subunit beta;Pdhb;ortholog	bound, repressed	Drosphila embryo (Chen et al., 2014)
RedOx homestasis	Thioredoxin domain-containing protein;DmelCG8993;ortholog	bound, repressed	Drosphila embryo (Chen et al., 2014)
TCA	Iso_dh domain-containing protein;DmelCG5028;ortholog	bound, repressed	Drosphila embryo (Chen et al., 2014)
tRNA metabolism	Tryptophanyl-tRNA synthetase;TrpRS-m;ortholog	bound, repressed	Drosphila embryo (Chen et al., 2014)
channel	Voltage-dependent anion-selective channel;porin;ortholog	bound	Drosphila embryo (Chen et al., 2014)
ETC	GH01077p;UQCR-C1;ortholog	bound	Drosphila embryo (Chen et al., 2014)
ETC	AT02348p;UQCR-C2;ortholog	bound	Drosphila embryo (Chen et al., 2014)
ETC	GE011443p1;UQCR-6.4;ortholog	bound	Drosphila embryo (Chen et al., 2014)
fatty acid beta-oxidation	Uncharacterized protein;DmelCG9149;ortholog	bound	Drosphila embryo (Chen et al., 2014)
fatty acid beta-oxidation	FI09602p;GH07925p;ortholog	bound	Drosphila embryo (Chen et al., 2014)
metabolicenzyme	Aspartate aminotransferase;Got2;ortholog	bound	Drosphila embryo (Chen et al., 2014)
mis c	NFU1 iron-sulfur cluster scaffold homolog, mitochondrial;FlyBase:FBgn0052857;ortholog	bound	Drosphila embryo (Chen et al., 2014)
mitochondrial organization	Coiled-coil-helix-coiled-coil-helix domain containing 2, isoform A;Chchd2;ortholog	bound	Drosphila embryo (Chen et al., 2014)
mitochondrial translation	RH08992p;BcDNA:RH08992;ortholog	bound	Drosphila embryo (Chen et al., 2014)
mitochondrial translation	39S ribosomal protein L22, mitochondrial;mRpL22;ortholog	bound	Drosphila embryo (Chen et al., 2014)
mitochondrial translation	Mitochondrial ribosomal protein S2;mRpS2;ortholog	bound	Drosphila embryo (Chen et al., 2014)
OxPhos	Cytochrome coxidase subunit 7A, mitochondrial;COX7A;ortholog	bound	Drosphila embryo (Chen et al., 2014)
OxPhos	RE57459p;CG6922;ortholog	bound	Drosphila embryo (Chen et al., 2014)
protein import	Heat shock protein 60A;Hsp60A;ortholog	bound	Drosphila embryo (Chen et al., 2014)
protein import	Mitochondrial import inner membrane translocase subunit TIM50-C;ttm50;ortholog	bound	Drosphila embryo (Chen et al., 2014)
protein import	DNL-type domain-containing protein;DmelCG8206;ortholog	bound	Drosphila embryo (Chen et al., 2014)
pyruvate metabolic process	Pyruvate carboxylase;PCB;ortholog	bound	Drosphila embryo (Chen et al., 2014)
TCA	Probable isocitrate dehydrogenase [NAD] subunit alpha, mitochondrial;Idh3a;ortholog	bound	Drosphila embryo (Chen et al., 2014)
ETC complex I	NADH dehydrogenase (ubiquinone) 24 kDa subunit	bound	Drosophila adult thorax (Chartier et al., 2015)
ETC complex I	NADH dehydrogenase (ubiquinone) B8 subunit	bound	Drosophila adult thorax (Chartier et al., 2015)
ETC complex I	NADH dehydrogenase (ubiquinone) 75 kDa subunit	bound	Drosophila adult thorax (Chartier et al., 2015)
ETC complex II	Succinate dehydrogenase, subunit B (iron-sulfur)	bound	Drosophila adult thorax (Chartier et al., 2015)
ETC complex II	Succinate dehydrogenase, subunit A (flavoprotein)	bound	Drosophila adult thorax (Chartier et al., 2015)
ETC complex II	Succinate dehydrogenase, subunit D	bound	Drosophila adult thorax (Chartier et al., 2015)
ETC complex III	Rieske iron-sulfur protein	bound	Drosophila adult thorax (Chartier et al., 2015)
ETC complex III	Ubiquinol-cytochrome c reductase	bound	Drosophila adult thorax (Chartier et al., 2015)
ETC complex IV	Cytochrome coxidase subunit 7C	bound	Drosophila adult thorax (Chartier et al., 2015)
ETC complex IV	Cytochrome coxidase subunit 7A	bound	Drosophila adult thorax (Chartier et al., 2015)
ETC complex V	ATP synthase, β subunit	bound	Drosophila adult thorax (Chartier et al., 2015)
ETC complex V	ATP synthase, subunit F	bound	Drosophila adult thorax (Chartier et al., 2015)

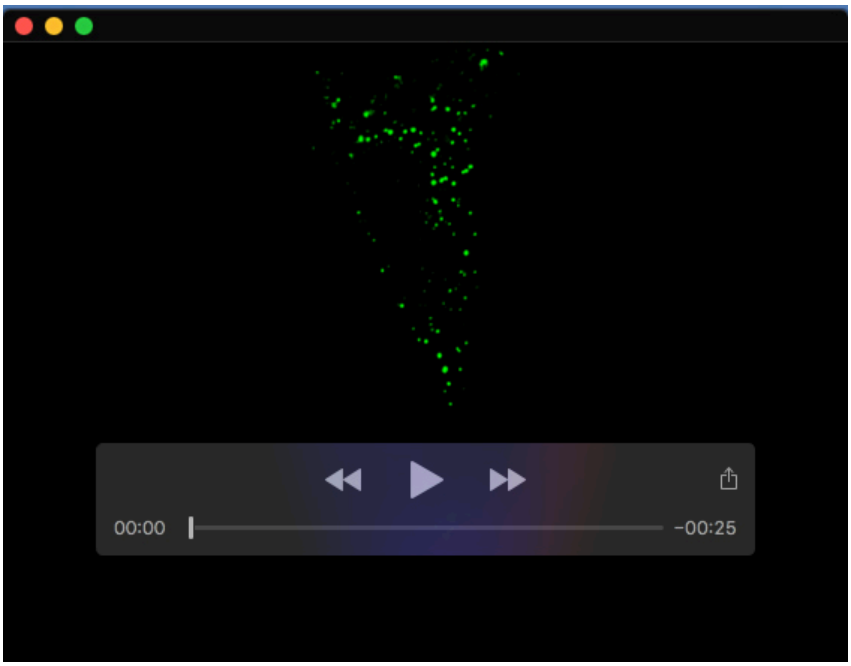

Movie 1. Live cell imaging of the Smaug1-EYFP expressing cell depicted in Figure 1A recorded during 30 min (0.5 frames per minute) as described in Materials and Methods.

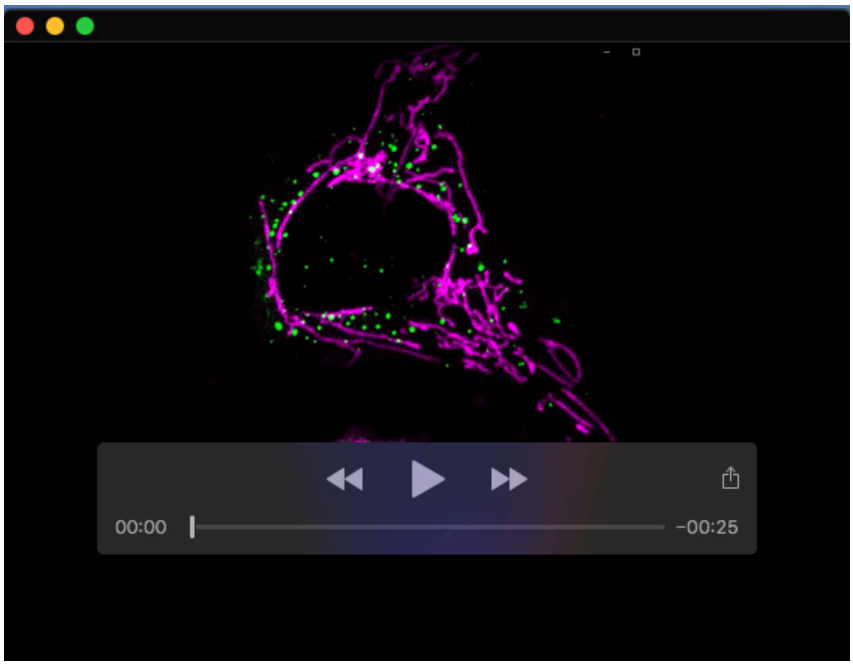

Movie 2. Live cell imaging of the control cell depicted in Figure 8A. Smaug1-EYFP (green) and Mito-dsRED (magenta) were co-transfected. One frame each 2 min during 32 min.

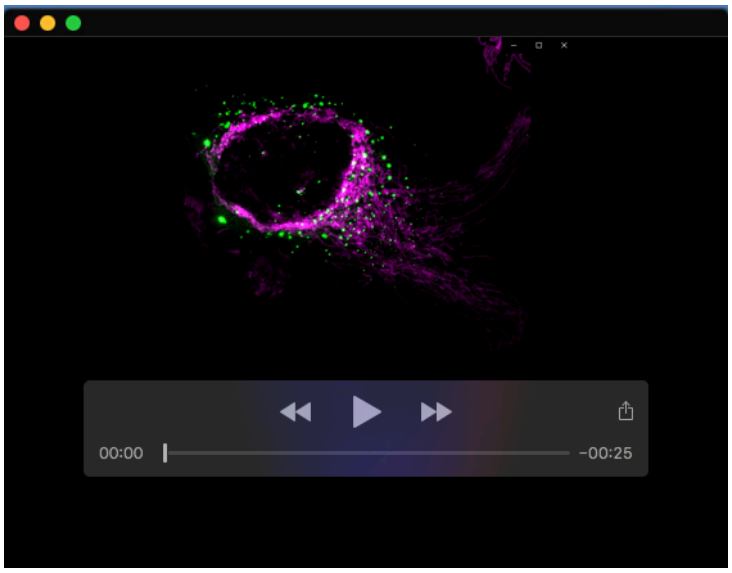

Movie 3. Live cell imaging of the metformin-exposed cell depicted in Figure 8A. Smaug1-EYFP (green) and Mito-dsRED (magenta) were co-transfected. One frame each 2 min during 32 min.